Evolution of disorder in magnetic stripe domains. I. Transverse instabilities and disclination unbinding in lamellar patterns

M. Seul and R. Wolfe
AT&T Bell Laboratories, Murray Hill, New Jersey 07974
(Received 13 May 1992)

Video polarization microscopy, optical diffraction, and digital image analysis have been employed to investigate the transformation of a well-ordered lamellar ("smectic") domain phase of ferrimagnetic garnet films into a globally disordered, "labyrinthine" pattern. Surprisingly, in view of the presence of nonlocal interactions, the ensuing pattern evolution in response to temperature-induced strain is characterized, in its first stages, by a (local) transverse elastic response which manifests itself in the form of "smectic" instabilities and generates undulation and chevron ("zigzag") patterns. At a characteristic limit of accumulated strain, the nucleation of topological defects in the form of disclination dipoles initiates the second stage of the evolution. The subsequent continuous, topologically constrained "unbinding" of these dipoles represents the essential mechanism mediating the loss of global orientational order in the pattern. The application of a set of algorithms for line-pattern analysis to track the motion of individual topological charges permits the quantitative description of this process. The emerging labyrinthine patterns represent the result of a constrained optimization and, while globally disordered, have in fact been shown to exhibit a robust and well-defined local structure in the form of "cybotactic" clusters.

PACS number(s): 64.60.−i, 05.70.Fh, 64.70.−p, 75.70.Kw

I. INTRODUCTION

A. Modulated phases

The idea that competing interactions favor the appearance of modulated phases has been fruitfully employed to yield mean-field descriptions of a wide variety of condensed-matter systems in two and three dimensions [1]. The unidirectional modulation of the appropriate order-parameter field constitutes the simplest possible realization of such a modulated phase, and stripe morphologies are in fact commonly encountered in diverse circumstances, including realizations in thin films of ferroelectrics [2], type-I superconductors [3], ferrofluids [4] and magnetic garnets [5], as well as in monomolecular amphiphilic films adsorbed at an air-water interface [6]. Very frequently, the observed stripe phases are disordered, a "labyrinthine" morphology predominating, and a stripe liquid having been observed recently in Langmuir monolayers [7]. Given the unifying nature of the description in terms of modulated phases, significant similarities among pattern morphologies in the various representative systems are to be expected, and the question arises as to the mechanisms underlying the evolution of disordered patterns. The effectively two-dimensional realizations of stripe patterns in Langmuir and magnetic garnet films offer the advantage of facilitating identification of topological (point) defects and analysis of their role in the disordering process. The results of such an investigation, undertaken with the aid of optical polarization microscopy and extensive digital pattern analysis on magnetic garnet films, will be described in the present and in the following article, referred to as II in what follows. Brief accounts of parts of this work have been previously given [8,9].

The evolution of labyrinthine patterns along two mutually orthogonal trajectories has been analyzed in detail. In II we investigate the processes mediating pattern evolution in response to demagnetization at a fixed temperature from a state of saturated magnetization. In the present article we report the results of a systematic analysis of the mechanisms by which globally disordered stripe domain states in ferrimagnetic garnet films evolve from a well-defined initial state in the form of an ordered lamellar pattern, realized at zero net magnetization. We rely on the extensive application of algorithms for line-pattern analysis to elucidate the essential role played by "nucleation" and "unbinding" of defect pairs in this process. The evolution of disorder is driven by strain, imposed on a given pattern by means of tuning the characteristic modulation wave vector via its temperature dependence.

B. Summary and outline

In II it is shown that field-induced pattern evolution from an initial state of homogeneous magnetization leads to a labyrinthine pattern via the elongation of a single (or a few) meandering stripe(s) of the invading ("minority") component, consisting of reverse-magnetized domain(s), confining topological defects completely to the "majority" component [9,10]. The resulting disordered state appears to represent a deep local minimum in the free energy of the stripe pattern which is reached under "adiabatic" conditions of increasing strain whenever topological constraints prevent access to the lamellar pattern representing the state of globally minimal free energy [9,10]. In contrast, the proliferation of defects in the domain pattern by continued nucleation predominates in response to rapidly increasing, magnetic-field-induced

strain, favoring the formation of highly branched stripe configurations. Striking "comb" patterns, composed of ordered arrays of alternating disclination dipoles, are observed in this situation. These findings suggest the existence of distinct classes of disordered structures, distinguished by the relative preponderance of branching over defect-dipole-unbinding events in the course of disordering.

In the present article we focus on the evolution of disorder in response to temperature-induced strain, following a trajectory along the symmetry axis ($H=0$) of the phase diagram. Our principal observations may be summarized as follows.

Starting with a lamellar state, prepared at a temperature T_0 and magnetic field $H=0$, temperature-induced strain triggers a sequence of "smectic" instabilities, consistent with a local elastic response of the pattern. The first instability is a transverse undulation, characterized by a single mode in the optical diffraction spectrum. Within the framework of an effective elastic theory, discussed in Sec. III, the corresponding period is set by effective curvature and compression moduli. A continuous addition of further modes of transverse distortion transforms the "curvature walls" of the undulation pattern into the "discontinuity walls" characterizing chevron ("zigzag") patterns [11]. This accommodation of increasing dilative strain culminates in the nucleation of topological defect pairs in the form of disclination dipoles, indicative of stripe or line branching. Under conditions of slowly increasing strain, existing disclination dipoles undergo a continuous "unbinding" transition. This entails the motion of disclinations of opposite charge, initially paired into a dipole, to uncorrelated positions and is described in detail in II.

Disclination dipole unbinding leads to the appearance of a globally disordered, labyrinthine state with a well-defined local structure. This is based on a prominent motif in the form of oblong polygonal clusters of ordered stripe segments [9]. Labyrinthine patterns display a characteristic density, n_D of disclinations defining an "intermediate" length scale $\xi \sim n_D^{-1/2}$, related to the characteristic size of segment clusters. As shown elsewhere [10], extensive statistical analysis of numerous structural attributes of such segment clusters reveals these to be remarkably robust and independent of the choice of trajectory in the magnetic-field–temperature phase diagram.

The remainder of this article adheres to the following outline: Sec. II contains a brief summary of experimental aspects which are more fully described in article II; a detailed discussion of the methods of digital image and pattern analysis employed here is given elsewhere [10]. In Sec. III we review the theoretical concepts providing the context for the discussion of our results. Section IV contains the bulk of our observations pertaining to the evolution of disordered patterns from a lamellar initial state in response to slowly varying, temperature-induced strain. The discussion of these findings in Sec. V is largely limited to the transverse instabilities of the lamellar pattern, arguing for the validity of a description in terms of a local "smectic" elastic Hamiltonian. A full discussion of the defect-mediated evolution of disorder, based on the entirety of pertinent results, is contained in II. This is guided by references to concepts from the theory of defect-mediated melting as well as to the description of amorphous structure.

II. EXPERIMENTAL PROCEDURES

A detailed account of experimental procedures is given in II. A brief summary of pertinent aspects is included here for the sake of completeness.

Experiments were performed on thin, transparent films of magnetic garnet of composition $(YGdTm)_3(FeGa)_6O_{12}$, grown on single-crystal substrates of gadolinium gallium garnet (GGG) of (111) orientation to a thickness of about 13 μm. The field required to saturate the films parallel to the surface is a factor of about 30 larger than the perpendicular saturation field. The films therefore exhibit the behavior of an Ising ferromagnet over a wide temperature range, with alternating domains of "up" and "down" magnetization in the characteristic "stripe" and "bubble" configurations.

Samples were placed into a small, temperature-controlled ceramic furnace of cylindrical shape, equipped on top and bottom with double-paned windows (Meadowlark Optics, Longmont, CO). The furnace was designed to fit into the 1-$\frac{1}{2}$-in.-diam bore of an air-cooled solenoid of 2-$\frac{1}{2}$ in. length, capable of generating an axial magnetic field of up to approximately 500 Oe. The entire assembly was placed on a stage to fit a standard Zeiss Universal microscope, equipped for polarization microscopy. Domains of magnetization were illuminated in transmission with polarized light, contrast resulting from the Faraday effect. A charge-coupled-device (CCD) video camera with external control of gain and black level (CCD 72, Dage MTI, Michigan City, IN) served to record images which were stored for later analysis on a video cassette recorder (Sony VO5800H, Sony Corp., Secaucus, NJ).

Diffraction spectra were recorded by imaging the depolarized component of the input illumination, in this case provided by the 514-nm line of an argon-ion laser (Innova 90-5, Coherent, Palo Alto, CA), in the back focal plane of a 10× objective of numerical aperature 0.3. This is accomplished by means of a Bertrand lens inserted in the optical train of the microscope. The spectra were recorded with a silicon intensified target (SIT) video camera (Cohu 5650, Cohu, San Diego, CA).

Computer control of all measurement and video-recording functions allowed for convenient and reproducible ramping of temperatures and magnetic fields and the capture of images as well as experimental parameters on video tape for subsequent analysis [12].

III. THEORETICAL CONTEXT

A. Theory of modulated phases: stripe and bubble domains in magnetic garnet films

Modulated phases appear in a number of condensed-matter systems under a variety of circumstances. In the smectic or analogous lamellar phases of liquid crystals [11] and amphiphilic materials such as phospholipids [13]

and in diblock copolymers [14], the characteristic modulation period is determined by molecular dimensions. Of particular interest in the present context are those instances in which it is the competition of short-ranged attractive and long-ranged repulsive interactions which gives rise to the modulation of the order-parameter field and the concomitant domain formation. Ferroelectrics [2], ferrofluidic layers [4,15], monomolecular amphiphilic ("Langmuir") films confined to an air-water interface [6,7] and the ferrimagnetic garnet films considered here [5,16] fall into this category. In all of these cases, a local, attractive interaction giving rise to a domain-wall energy or line tension, is balanced by a nonlocal repulsive contribution to the free energy which is of electrostatic or magnetostatic origin. Related theories of a mean-field type, all based on this general idea, have been advanced to account for domain formation in all the aforementioned systems. A similar argument has also been invoked to construct an elastic theory for the steps on vicinal surfaces of semiconductors; it is again based on the concept of competing interactions, the repulsive part arising from (generally anisotropic) strain [17].

Pertinent to the present discussion is the theoretical analysis of domain formation formulated by Garel and Doniach in which a thin uniaxial magnetic garnet film is represented as a dipolar Ising ferromagnet [18]. Specifically, the theory is based on a free energy of the type

$$F \sim \int d^2r (f_{\rm attr} + f_{\rm rep}) .$$

Here, the attractive part, reflecting the ferromagnetic exchange coupling between neighboring spins, determines the energy of the domain wall separating domains of opposite magnetization. The repulsive component, arising from (sample shape-dependent) demagnetizing fields, is modeled in the form of an additional dipolar interaction between spins. Within the framework of a Ginzburg-Landau treatment, the theory thus takes the following form for a system assumed to be isotropic within the plane of the film [18]. It contains an attractive part,

$$f_{\rm attr} = \frac{D}{2a} J (\nabla m)^2 + \frac{D}{a^3}(T - T_c)\frac{m^2}{2} + \frac{DT_c}{12a^3} m^4 - \mu_B g \frac{D}{a^3} mH ,$$

where a, D, J, $T_c \sim J$, m, and H, respectively, represent the (microscopic) lattice constant of the garnet, the thickness of the film, the nearest-neighbor ferromagnetic exchange, the mean-field ferromagnetic transition temperature, the layer magnetization $m = (0,0,m)$, oriented normal to the plane of the film, and the external (axial) magnetic field. Balancing $f_{\rm attr}$ is a repulsive contribution of the form

$$f_{\rm rep} = \tfrac{1}{2} \int d^2r' m(r) g(r,r') m(r') ,$$

where the kernel $g(r,r')$ incorporates dipolar interactions:

$$g(r,r') = (\mu_B g)^2 \int dq \frac{4\pi}{q} (1 - e^{-qD}) e^{iq(r-r')} .$$

The gradient-square term in $f_{\rm attr}$ represents the energy penalty incurred by introducing a domain wall. It is equivalent to a line tension and balances the tendency of continued domain subdivision favored by the repulsive term, because that process requires the proliferation of domain walls. One therefore expects the appearance of a new length scale, the modulation period $d \equiv 2\pi/q_0$ of the intralayer magnetization which is determined by the relative strengths of domain-wall and dipolar energies. Within a single-mode approximation, assumed to be valid near the (mean-field) critical point and in the limit $q_0 D \gg 1$, implying $e^{-q_0 D} \simeq 0$, the theory gives

$$q_0 = \left[2\pi \frac{(\mu_B g)^2}{JD} \right]^{1/3} .$$

The exponent of $\frac{1}{3}$ is the consequence of relying on a single-mode approximation and the assumption $q_0 D \gg 1$, the solution for the full square-wave profile yielding an exponent of $\frac{1}{2}$ [19,20]. Irrespective of this detail, the expression is entirely consistent with the qualitative argument just given: The relative strengths of dipolar $[(\mu_B g)^2]$ and domain-wall (J) coupling terms determine q_0, strong dipolar interactions favoring a small stripe period, $d_0 = 2\pi/q_0$; note also that in the expression just given, q_0 is independent of the external field H.

The field dependence of the stripe period, $d = d_T(H)$, has been determined numerically from the complete solution for the magnetostatic potential of a set of parallel stripe domains of alternating magnetization [5,21,22]; for convenience of reference, a graph of the solution given by Kooy and Enz [5] is reproduced as part of Fig. 1. A scaling prediction for the temperature dependence of the modulation period, $d = d_H(T)$, $T < T_c$, is also available [20]. As will be discussed in greater detail elsewhere [23], Barker and Gehring [20] combine the result [24] $d \sim (\sigma D / m_0^2)^{1/2}$ for a square magnetization profile of amplitude $\pm m_0$ with the temperature dependence $\sigma \sim m_0^2 |T - T_c|^{1/2}$ for the energy of a domain wall of the Ising type [25]. For temperatures $T < T_c$, this leads to the prediction $d \sim |T - T_c|^{1/4}$, expected to be valid as long as adjacent domain walls do not interact, i.e., in a regime approaching (but not actually attaining) a limit equivalent to "weak segregation," familiar in the context of phase-separation theory.

Note that the cited temperature dependence implies the *decrease* of the stripe period with increasing temperature. This situation, somewhat counterintuitive at first sight, arises as a result of the fact that the long-range dipolar interaction is expected to scale with temperature in the same way as the order parameter, $m_0 \sim |T - T_c|^{\beta}$, $\beta = \frac{1}{2}$, while the domain-wall (or line-tension) term vanishes more rapidly, $\sigma \sim |T - T_c|^{\mu}$, $\mu > \beta$. Consequently, the dipolar repulsion predominates as the mean-field critical point is approached, favoring the proliferation of domain walls.

Interestingly, the qualitative argument just sketched to rationalize the predominance of dipolar interactions as T_c is approached is analogous to that advanced to postulate the existence of critical-point wetting [26]. Consider-

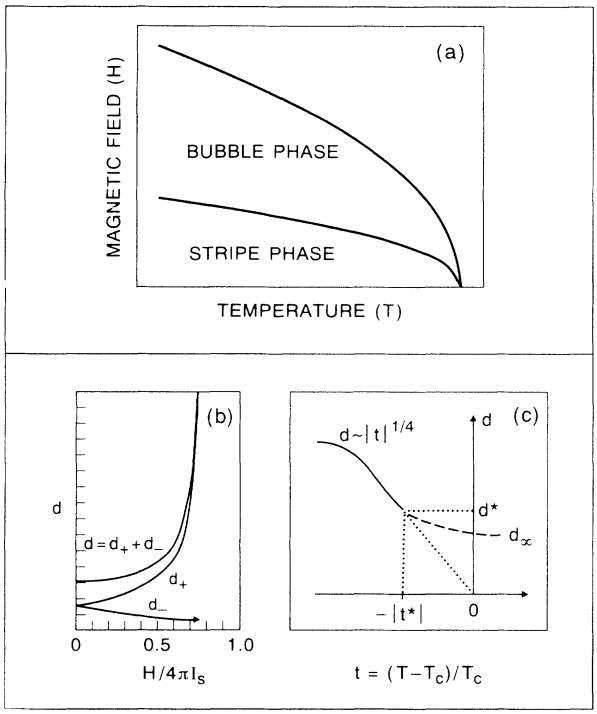

FIG. 1. Upper panel (a): mean-field phase diagram of the dipolar Ising ferromagnet exhibiting, respectively, the trigonally and unidirectionally modulated "bubble" and "stripe" phases. First-order transition lines are shown to meet in a critical point. The drawing is adapted from Fig. 3 of Ref. [18]. Lower panel, left-hand side (b): magnetic-field dependence of the stripe period, $d=d_T(H)$, at fixed temperature T; also shown is the field dependence of the respective thicknesses of majority $[d_+(H)]$ and minority $[d_-(H)]$ phases where $d=d_+ + d_-$. The drawing is adapted from Fig. 15 of Ref. [5]. Lower panel, right-hand side (c): temperature dependence of the stripe period, $d=d_H(T)$, at fixed magnetic field H. The drawing is adapted from Fig. 5 of Ref. [20].

ing, for example, a solid phase s in contact with two fluid phases α and β, one generally has $\sigma_{\alpha\beta} \geq |\sigma_{\alpha s} - \sigma_{\beta s}|$, σ denoting surface tension. As the critical point, $T_c^{(\alpha,\beta)}$, is approached, both $\sigma_{\alpha\beta}$ and $\sigma_{\alpha s} - \sigma_{\beta s}$ vanish; however, as before, $\sigma_{\alpha\beta}$ vanishes more rapidly, $\sigma_{\alpha\beta} \sim |T - T_c^{(\alpha\beta)}|^{\mu}$, than does $\sigma_{\alpha s} - \sigma_{\beta s} \sim |T - T_c^{(\alpha\beta)}|^{\beta}$. As a result, the equality $\sigma_{\alpha\beta} = \sigma_{\alpha s} - \sigma_{\beta s}$ will be satisfied, and a wetting transition must therefore occur, before $T_c^{(\alpha\beta)}$ is actually attained, and one of the fluid phases, β, say, completely wets the solid, intruding between s and α so that $\sigma_{\alpha s} = \sigma_{\beta s} + \sigma_{\alpha\beta}$.

The phase diagram derived on the basis of mean-field theory from the energy functional just discussed is reproduced in Fig. 1 and exhibits unidirectionally modulated ("stripe") and triagonally modulated ("bubble") phases exemplified by the patterns in Fig. 2. The first-order-transition lines separating stripe, bubble, and homogeneous, that is, completely magnetized, phases are expected to meet in a critical point [18]. The actual existence of this critical point remains open to question, and is an issue we will discuss elsewhere in more detail [23].

Aside from continuing interest in the domain structure of magnetic garnets motivated by potential technological applications [27–29], a variety of problems involving topological considerations have been recently pursued in connection with stripe and bubble domains. These include the coarsening of cellular-domain networks [30,31], closely related to the analogous phenomenon in soap froths [32]; the study of two-dimensional melting of the "hexagonal" bubble phase whose ordered state was in fact found to lack long-range positional order due to random impurities [33]; the observation of discommensurations in lamellar stripe patterns formed in garnet films whose thickness D was modulated so as to favor differing values of the stripe period [34]; and the topological hysteresis experienced by stripe patterns subjected to a variety of magnetic-field cycles [35]. The type of pattern evolution reported by the latter group of authors is of particular interest in the present context. Another reference point is the existence in a Langmuir film of what we have referred to as a two-dimensional "stripe liquid" [7].

To investigate the elastic properties of a collection of magnetic stripes, Garel and Doniach [18] model the response of this system by a harmonic expansion in the displacements away from the selected optimal modulation period, $d_0 = 2\pi/q_0$. As detailed by Sornette [19], the phase approximation

$$m(r) = m_0 \cos\{q_0[x - u(x,y)]\}$$

for the x-modulated magnetization $m(r)$, $u = u(x,y)$ representing the stripe displacement field, eventually yields, up to quadratic order in u, an effective smectic elastic free energy of the well-known form [11,36,37]

$$F(K,B) = \int d^2r [\tfrac{1}{2}B(\partial_u x)^2 + \tfrac{1}{2}K(\partial_u^2 y)^2] ,$$

where K and B, respectively, represent effective curvature and compression moduli; they are given by [19]

$$K = \frac{2JD}{a} m_0^2 ,$$

$$B = 8\frac{JD}{a} m_0^2 q_0^2 ,$$

so that the "penetration depth" [11] $\lambda = \sqrt{K/B}$ becomes $\lambda = \frac{1}{2}q_0 = d_0/4\pi$. A peculiarity of this smectic free energy is the anisotropy of its elastic response to transverse undulation modes, restored only by curvature and characterized by relatively low excitation energy, as opposed to longitudinal layer compression modes of higher energy. As a result, bending of layers is generally favored over compression. This anisotropy also manifests itself in anisotropic scaling of positional correlations near the disclination-unbinding transition of two-dimensional stripes into the isotropic phase [37].

Helfrich discovered that thermally excited undulations of sufficient amplitude will lead to entropic repulsion between adjacent layers in lamellar arrangements [38]. This prediction has in fact been confirmed experimentally in ternary surfactant mixtures [39]. In contrast, magnetic

stripes are expected to exhibit a very substantial bending stiffness: Sornette [19] gives an estimate of $K \simeq 10^3 kT_c$, T_c denoting the mean-field ferromagnetic transition temperature. Entirely consistent with this expectation is the absence of any readily observable effects of thermal fluctuations over most of the experimental phase diagram [23,35]. A significant bending stiffness implies a macroscopic range of smectic positional correlations in magnetic systems. Given the pertinent expression for $\langle m(r)m(0)\rangle$ derived by Toner and Nelson (Eq. 1.8 in Ref. 36), the transverse correlation length has the form $\xi_\perp = 4B\lambda/q_0^2 kT$, and with $\lambda^2 = K/B = \frac{1}{4}q_0^2$, one finds $\xi_\perp = (d_0/4\pi)(K/kT)$; given the cited estimate $K \simeq 10^3 kT$, this implies $\xi_\perp \simeq 10^3 d_0$. For our experiments, a typical value for d_0 of 10 μm yields correlation lengths $\xi_\parallel > \xi_\perp$ of the order of millimeters. Clearly, it would be difficult to assess the predicted exponential decay of positional correlations for a two-dimensional smectic phase in any magnetic film of practical size. The smectic elastic theory of magnetic stripe domain phases advocated by Sornette [19] accounts well for a variety of "smectic" pattern instabilities as well as defect formation. We return to it in the discussion of our results on strain-induced stripe-phase disordering in Sec. V.

B. Topological defects, melting, and amorphous structure

A question of fundamental importance to the understanding of structural disorder and its evolution has surrounded the role of topological defects. Long considered essential in this context [40], topological defects are explicitly invoked in analytical theories of melting in two dimensions which connect the appearance of free topological charges to the disruption of long-range translational and orientational correlations. A great deal of experimental and computational effort has been directed at the elucidation of the novel hexatic phase predicted in these theories, an orientationally ordered phase of a trigonally symmetric two-dimensional condensate which contains a finite density of free dislocations and exhibits an exponential decay of translational, but a slower, algebraic decay of orientational correlations [41]. The theoretical analysis has been extended to anisotropic [42] and to unidirectionally modulated, "smectic" or "lamellar" phases in two dimensions [36,37]. Commonly observed in thermotropic and lyotropic liquid crystals and related materials [13,14] and known to display a lower marginal dimension of $d=3$ and hence algebraically decaying translational correlations [43], smectic phases in three dimensions have been the subject of extensive study. In two dimensions, theory predicts the unbinding of dislocations to occur at $T=0$, implying the existence of a finite density of free dislocations at all finite temperatures ($T>0$) [18]. Given the twofold symmetry of the unidirectionally modulated state, one expects the formation of a two-dimensional "nematic" phase [37,44] characterized, in analogy to the hexatic phase, by the exponential decay of translational and algebraic decay of orientational correlations. Specifically, this phase is envisaged to be populated by a density of free dislocations, separated by a characteristic distance $\xi_D \sim n_D^{-1/2}$. On length scales less than ξ_D, smectic order is realized; the ordered regions, or "cybotactic clusters," attain a characteristic size and eccentricity, such that $L \sim \xi_D^{4/3}$, $W \sim \xi_D^{2/3}$, and $A \sim \xi_D^2$; L, W, and A, respectively, denote cluster length, width, and area. On length scales exceeding ξ_D, nematic ordering of cybotactic clusters obtains. The appearance of the isotropic liquid is thought to be mediated by the unbinding of disclination pairs [36]. Attempts to investigate the melting of two-dimensional stripe phases experimentally have been few, partly as a consequence of the limited number of systems which are suitable for requisite measurements and which exhibit such phases and their melting transition [45–47].

Topological defects also represent a prominent feature of amorphous structures. It has been suggested that their ubiquitous appearance is a consequence of topological "frustration." This arises when local chemical ordering generates a packing arrangement in the form of a regular polyhedron, such as the tetrahedron favored in metallic systems, which does not permit the tesselation of three-dimensional Euclidean space and is therefore inconsistent with long-range translational ordering [48,49]. This frustration, generic to amorphous structures, may be alleviated by permitting the embedding space to curve, thereby enabling the formation of periodic arrangements in accord with local packing requirements. In this picture, networks of disclination lines appear in the process of mapping the periodic structure constructed in an appropriately chosen curved space into Euclidean space [48]. Alternatively, the defect lines may be viewed as a natural consequence of the curvature mismatch between the curved space permitting tesselation and ordinary Euclidean (flat) space [49].

To construct explicit structural models for amorphous structures, one of two descriptive frameworks is frequently invoked. In the case of covalent glasses, preference is normally given to the continuous-random-network (CRN) picture, while a random-close-packing (RCP) representation is favored in connection with elemental (metallic) glasses. Given that a random-packing representation generates an associated random network via Voronoi tesselation, these two modes of description are in fact complementary in this sense [50]. The network representation reveals a characteristic feature of amorphous structures in the form of rings (or cells) containing an odd number of bonds (or faces). The disclination (or "odd") lines associated with odd-numbered rings figures prominently in a recent attempt to develop a general theoretical treatment of glasses, adopting the point of view that "odd" lines in fact constitute a central element of random matter [51,52].

A universal structural attribute of glasses manifests itself in diffraction measurements on a diverse variety of such materials in the form of a prominent peak in the structure factor, $S(q)$, at low values of the momentum transfer, q. This feature indicates that glasses, while by definition failing to achieve long-range ordering, nevertheless exhibit ordering on intermediate length scales exceeding the first few nearest-neighbor distances [53,54].

IV. EVOLUTION OF DISORDER IN LAMELLAR STRIPE DOMAIN PATTERNS: DISORDERING IN RESPONSE TO TEMPERATURE-INDUCED STRAIN

In this section we investigate the disordering of an initial state displaying well-defined smectic or lamellar ordering, exemplified by Fig. 2. In all experiments analyzed here, as well as in II, disordering is driven by externally imposed strain. While this is controlled via the temperature [20,23] and, as discussed in II, via the magnetic-field [5] dependence of the characteristic modulation wave vector, $q=q(H,T)$, described in Sec. I B, it is important to note that, over the range of parameters relevant to the present report, temperature is otherwise not a relevant variable. That is, no fluctuation effects are in evidence, in contrast to what is observed in the "critical" region [23] and at distinct variance with the fluctuation-dominated behavior of the stripe phase currently under study in certain Langmuir films [7].

In particular, we investigate in what follows the disordering process along the $H=0$ symmetry axis of the mean-field phase diagram, sketched in Fig. 1. By symmetry, the net magnetization

$$m \equiv (M_{\uparrow} - M_{\downarrow})/(M_{\uparrow} + M_{\downarrow})$$

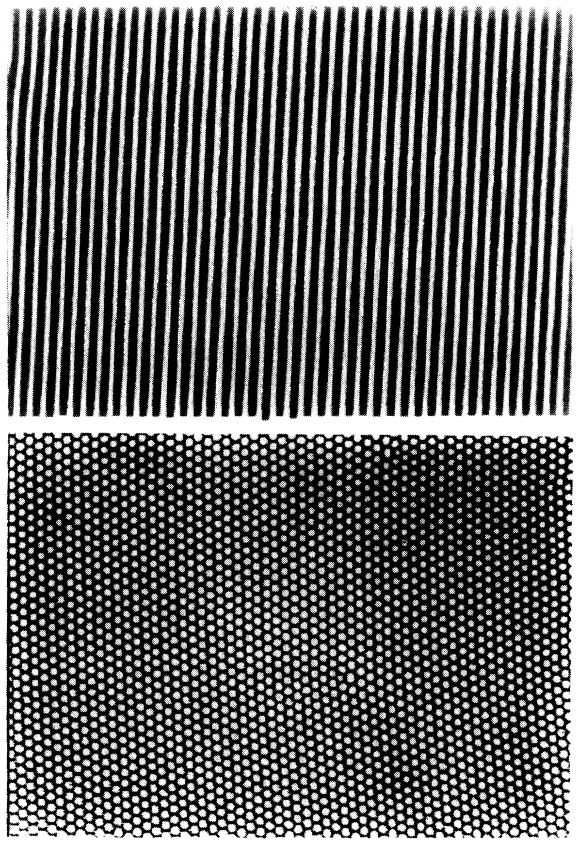

FIG. 2. Experimental examples of (spontaneously formed) "stripe" and "bubble" phases, recorded in a ferrimagnetic garnet film of the type investigated here and described in Sec. II of the text. Field and temperature settings were $H=0$ Oe, $T \simeq 0.6 T_c$ and $H=5$ Oe, $T \simeq 0.9 T_c$, respectively, for stripe and bubble patterns; $T_c \simeq 192$ °C. The horizontal dimension of the field of view is 570 μm in both cases.

vanishes on this line: $m=0$. Invoking digital line-pattern analysis, we examine in detail the formation and eventual unbinding of disclination dipoles, the process mediating the formation of globally disordered "labyrinthine" patterns. An abbreviated account of some of the results to be presented here has been given previously [8].

A. Transverse (smectic) instabilities

Along the $H=0$ axis, the modulation wave vector $q=q_{H=0}(T)$, and hence the stripe period $d=d_{H=0}(T)$, may be tuned via its temperature dependence, predicted to have the form shown in Fig. 1(c). We have investigated this dependence experimentally and find it to be in qualitative accord with the simple scaling prediction

$$d_{H=0}(T) \sim |T - T_c|^{1/4} ,$$

introduced in Sec. I B, although important deviations from this behavior have been observed in the vicinity of the "critical" point [23]. For the present purpose it suffices to realize that d does indeed exhibit a slow decrease with increasing temperature. It follows that the pattern may be expanded and compressed by moving along the $H=0$ axis, i.e., by, respectively, lowering or raising the temperature.

As pointed out by Molho, Porteseil, and Souche [34], a well-ordered lamellar pattern may be generated by cooling a garnet film from the "paramagnetic" state at $T > T_c$ through the phase transition in zero (normal) field, $H=0$. Unless special precautions are taken, small ($\lesssim \frac{1}{2}$ Oe) intralayer fields $H_{\parallel}$ will be present which break the azimuthal symmetry and aid alignment of the lamellar phase, a point discussed more thoroughly in the appropriate context of addressing the system's critical behavior [23].

Given the dependence of the stripe period d, the stripe pattern continues to expand or "coarsen," as T is lowered, necessitating the adjustment of the number N_L of lamellae present in the film. In a sample of linear dimension $L_0 = N_L d$, the "equilibrium" density $n_L \equiv N_L / L_0$ of lamellae is trivially seen to vary as $n_L \sim d^{-1}$.

The process by which the number of lamellae is decreased to accommodate the pattern coarsening induced by cooling along the $H=0$ axis is that of dislocation nucleation and climb, facilitating the "ejection" of lines from the sample; it is depicted in Fig. 3. The force acting on the free stripe end and thus facilitating defect motion results from the strain-induced curvature of lines adjacent to the defect; this Peach-Koehler force [11] has been recently analyzed in the present context by Sornette [19]. Although no quantitative study has been made, the process is closely related to the mechanism of period adjustment of rolls [55] in dynamical systems exhibiting a Rayleigh-Bénard instability. Bodenschatz (personal communication) has pointed out that, as with dynamical systems locked into a unidirectionally modulated ("roll") state, the lamellar magnetic pattern may also exhibit an Eckhaus instability [55] manifesting itself in the form of a longitudinal modulation of long wavelength, $\lambda_{\parallel} \gg d$, and corresponding satellite peaks at $q \pm \Delta q$ about the harmonics of

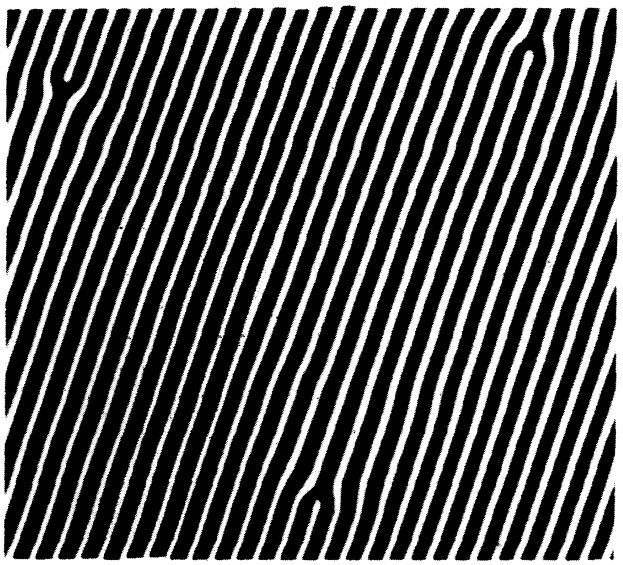

FIG. 3. Snapshot of dislocation climb, observed in the course of cooling a lamellar stripe pattern along the $H=0$ axis of the phase diagram of Fig. 1: This process of "ejecting" stripes enables the pattern to accommodate the increase in the stripe period induced by lowering the temperature, as discussed in Sec. IV A of the text. The horizontal dimension of the field of view is 930 μm; the stripe period is 32 μm.

$$q_{H=0}(T)=2\pi/d_{H=0}(T) ,$$

where $\Delta q=2\pi/\lambda_{\parallel}$. While this point may warrant closer attention, our existing Fourier spectra do not contain pertinent satellites, but may be resolution limited.

The ejection of lines is mediated by dislocation climb and thus involves domain-wall motion. It is therefore sensitive to domain-wall pinning by impurities, a process observed in samples with surface defects. In this situation, the application of an ac magnetic field H_{ac} of small amplitude can be useful, particularly at lower temperature. Importantly, the process of line ejection just described permits the system to remain in the lamellar state during coarsening along the $H=0$ axis between $T=T_c$ ($\simeq 192\,^{\circ}$C) and room temperature. It is readily apparent that there will be a sequence of unstrained "commensurate" states in which the actual number of lamellae exactly matches that dictated by the condition $N_L \cdot d \sim L_0$. Deviation of d from the corresponding value leads to the accumulation of strain and the eventual formation of defects and elimination of additional lamellae.

The coarsening process may be stopped at any temperature T_0 along the $H=0$ axis. We now proceed to examine the response to temperature-induced compression of the lamellar state, prepared at T_0 and $H=0$ and composed of a number $N_L \sim L_0/d_{H=0}(T_0)$ of lines (or lamellae). The argument $N_L \sim d^{-1}$ implies that, as d decreases with increasing T, N_L must be increased, necessitating the nucleation and "injection" of additional lines if the system is to remain in the lamellar state. However, the requisite process of nucleating new lamellae—that is, the converse of the generation of edge dislocations during coarsening—is generally not observed. Consequently, the temperature-mediated reduction of the stripe period, coupled with the constraint $m=0$, implies that the lamellae pattern accumulates dilative strain. To accommodate the required decrease in the stripe period, d, the system undergoes an undulation ("buckling") instability when a threshold $\hat{\epsilon}\equiv(d_0-d)/d_0$ in dilative strain is reached, $d_0\equiv d(T_0)$ denoting the period of the lamellar initial

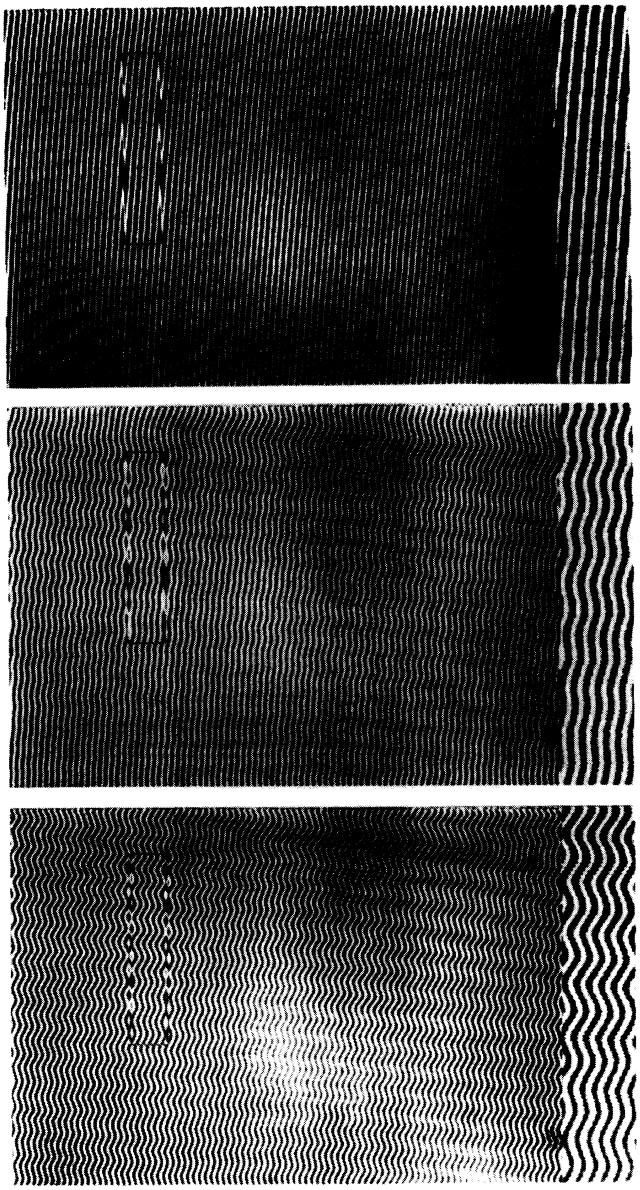

FIG. 4. Undulation instability of lamellar stripe pattern; the instability is induced by dilative strain, generated by heating along the $H=0$ axis of the phase diagram of Fig. 1(a). The lamellar initial state is displayed in the top panel. The transient depicted in the middle panel suggests that amplitude growth (along each undulating stripe) is continuous. The fully evolved undulation is shown in the bottom panel. The original images were processed by successive application of low-pass and high-pass filters. For clarity the vertical panel on the right-hand side of each figure depicts a twofold magnified view of the portion delineated by the rectangular box in the original. The horizontal dimension of the original field of view is 1.2 mm.

state. The inspection of transient states, obtained in the presence of a small lateral temperature and hence strain gradient, and illustrated in Fig. 4, suggests amplitude growth to be continuous, as expected on the basis of a linear stability analysis of the smectic free energy functional introduced in Sec. III A [19]. This analysis follows that first given in the context of the completely analogous, mechanically induced undulation instability of a (three-dimensional) smectic-A liquid crystal of N lamellae, confined between two glass plates [56,57]. This analysis also yields an expression for the new length scale introduced by the instability, namely, the transverse period, $\lambda_\perp \simeq \sqrt{\lambda L_0}$, where $\lambda \equiv \sqrt{K/B}$ is the penetration depth of Sec. III A.

From Fourier spectra of the type shown in Fig. 5, we find $q_\perp/q_0 \simeq \frac{1}{5}$ for the ratio of transverse and longitudinal

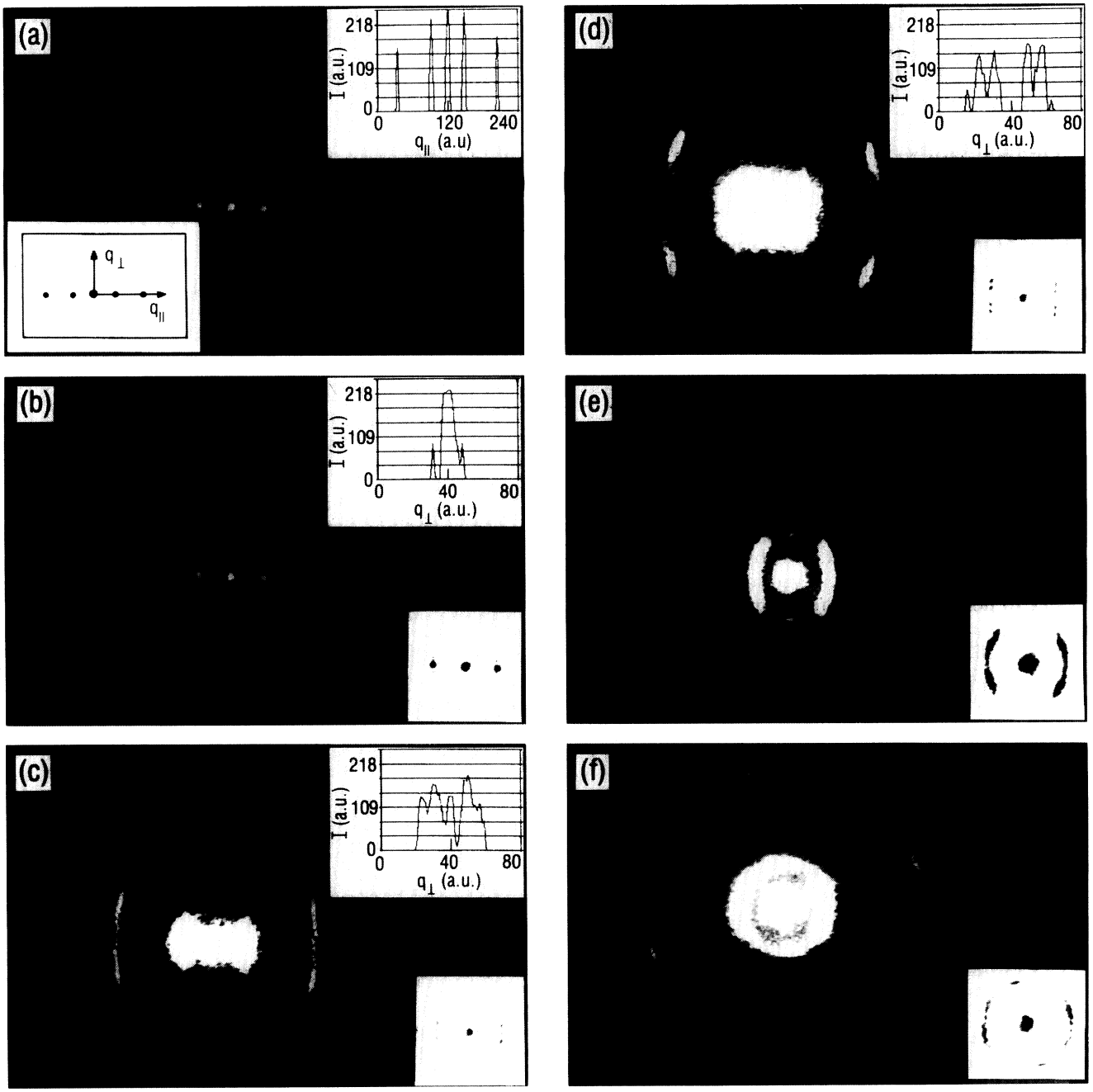

FIG. 5. Optical diffraction patterns characterizing transverse instability of lamellar pattern, the resulting undulation and chevron patterns, and the appearance of disclination dipoles and their subsequent unbinding (see further discussion in the text). The limiting ratio $q_\perp/q_\parallel = q_\perp/q_0 = 0.71$, realized in the chevron pattern giving rise to the spectrum in D, implies a substantial strain, $\epsilon = (d_0 - d)/d_0 = 1 - 1/[1 + (q_\perp/q_0)^2]^{1/2} = 0.18$. Insets contain resolved recordings of the central portion of the pattern in (b)–(f), as well as longitudinal (a) and transverse scans (b)–(d), the latter centered at the (10) position.

components of the modulation wave vector, implying $\lambda_\perp \simeq 2\times 5\times d_0$, where $d_0=2\pi/q_0$; hence,

$$\sqrt{\lambda L_0}=\sqrt{(d_0/4\pi)(N_L d_0)}=\sqrt{N_L/4\pi}\,d_0\simeq 10 d_0$$

and $N_L \simeq 1200$—that is, the instability involves the collective buckling of several hundred lamellae, occupying macroscopic portions of sample. The diffraction pattern in Fig. 5(b) reveals the instability to involve a single mode, as suggested by theory [19].

Further compression, inducing additional dilative strain, transforms the essentially sinusoidal undulation continuously into a chevron or "zigzag" pattern, shown in the top of panel Fig. 6. That is, the wide "curvature walls" of the undulation pattern contract into narrow "discontinuity walls" [11,19] characterized by a distinct tip in which the curvature energy is now concentrated. Optical diffraction patterns recorded in the course of this evolution and displayed in Figs. 5(c) and 5(d) reveal the appearance of higher transverse harmonics and the eventual disappearance of intensity in the longitudinal harmonics of the original lamellar pattern; the final state is characterized by a set of four off-axis spots with $q_\perp/q_0\simeq 0.71$ and thus an angle $\hat{\alpha}=(\pi-2\phi)$ subtended by the discontinuity walls where

$$\phi=\tan^{-1}(q_\perp/q_0)\simeq 35^\circ ,$$

as reported previously [8].

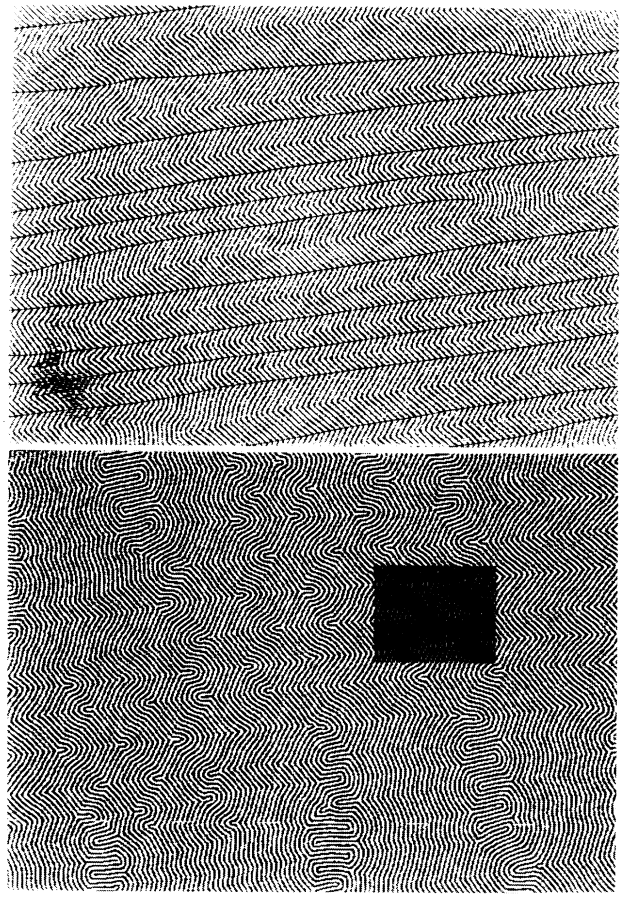

FIG. 6. Chevron pattern (top) and emerging disclination dipole pairs (bottom). Right-pointing cusps in the chevron pattern are connected by a thin line to guide the eye. The highlighted portion of the bottom photograph contains the medial axis transform [10], or "skeleton," of the white component and illustrates the appearance of rhombohedral tiles with defect-decorated vertices, as discussed in the text [(see also Fig. 8(d)]. The original images were processed by successive application of low-pass and high-pass filters. The horizontal dimension of the field of view is 1.4 mm.

As the modulation period continues to decrease with increasing temperature, the transverse period of the chevron also undergoes a period adjustment. As illustrated in Fig. 7, edge dislocations, also referred to as "metadislocations" [19], appear in the chevron superstructure. Their expulsion via climb can occasionally be observed: this process facilitates period adjustment in the chevron superstructure which is possible only in discrete steps, the stepsize being set by the prevailing transverse period. That is, the expulsion of edge dislocations in the chevron pattern serves to decrease the density of "crests," and this adjustment essentially leads to local "period doubling." Remarkably, the transverse modulation wavelength of the chevron thus tends to increase with decreasing modulation period d of the underlying stripe phase, in contrast to what would be expected from the dependence $\lambda_\perp \sim d$ derived from linear stability analysis. This observation is currently not accounted for by theory.

B. Nucleation and unbinding of topological defects

At a threshold of dilative strain,

$$\hat{\epsilon}=(d_0-d)/d_0=1-1/[1+(q_\perp/q_0)^2]^{1/2}\gtrsim 0.2 ,$$

the chevron pattern yields via nucleation of disclination dipoles emerging from the tips of the pattern. This process has been referred to as elementary pinch ("pincement") in the context of classifying fan-shaped textures in cholesteric mesophases [58,59]. As the lower panel of Fig. 6 as well as Fig. 8(d) demonstrate, dipoles are aligned in the direction of the ridges formed by discontinuity walls in the chevron pattern, that is, transverse to that of the original lamellar pattern. Furthermore, as discussed in detail in a related article [10], topological defects are essentially equally frequently formed in both bright and dark components of the patterns, as is apparent in Fig. 8(d). The appearance of disclinations in the chevron generates a new (approximate) local rotation symmetry, giving rise to a pseudosixfold diffraction pattern, as shown in Fig. 5(e). The diffraction spectra reveal that the original lamellar pattern of period $d_0=2\pi/q_0$ accommodates compression, in this instance temperature induced, by a transverse elastic response. The "buckling" of the pattern is seen to correspond to the addition of a transverse component $q_\perp$ to the modulation wave vector so that $\mathbf{q}=(q_\parallel,q_\perp)$; in particular, the longitudinal component $\mathbf{q}_\parallel$ remains unchanged from the value attained at the onset of the transverse instability: $\mathbf{q}_\parallel=\mathbf{q}_0$. That is, the distorted patterns realize the required reduction in the stripe period d, measured in the direction of the local stripe normal:

$$d=2\pi/(q_0^2+q_\perp^2)^{1/2}<d_0 .$$

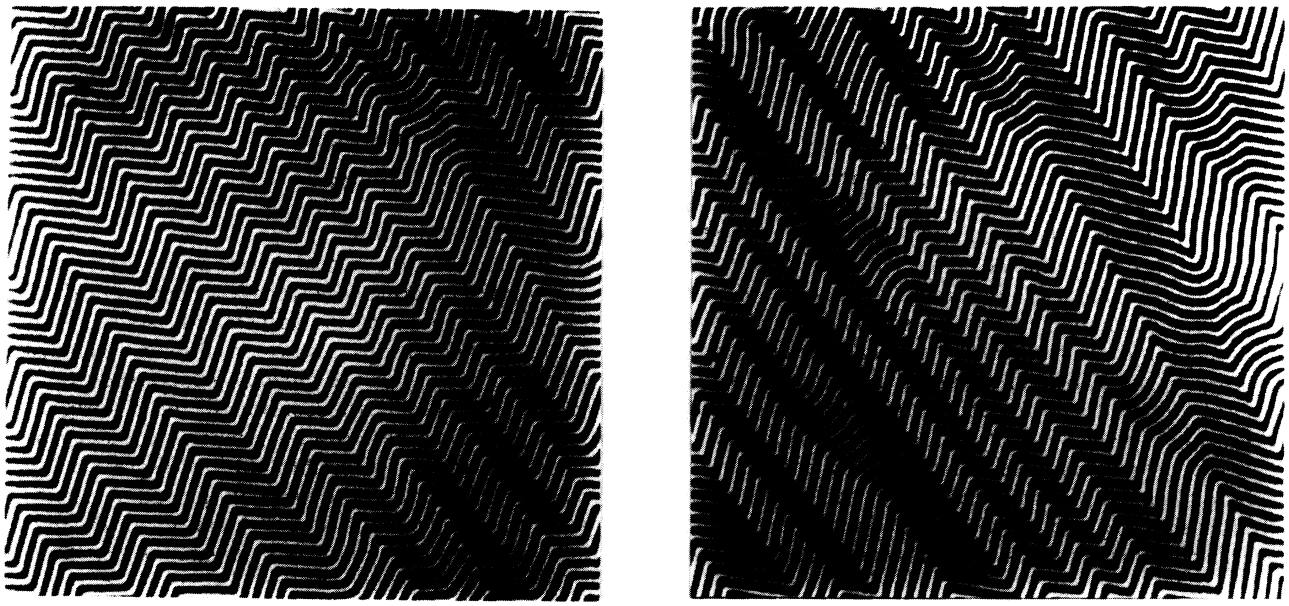

FIG. 7. Edge ("meta") dislocations in the array of discontinuity walls defining a chevron pattern of the type shown in the top panel of Fig. 6. These defects appear to mediate the period adjustment in the chevron pattern in a manner analogous to the process discussed in connection with Fig. 3. The horizontal dimension of each field of view is approximately 690 μm.

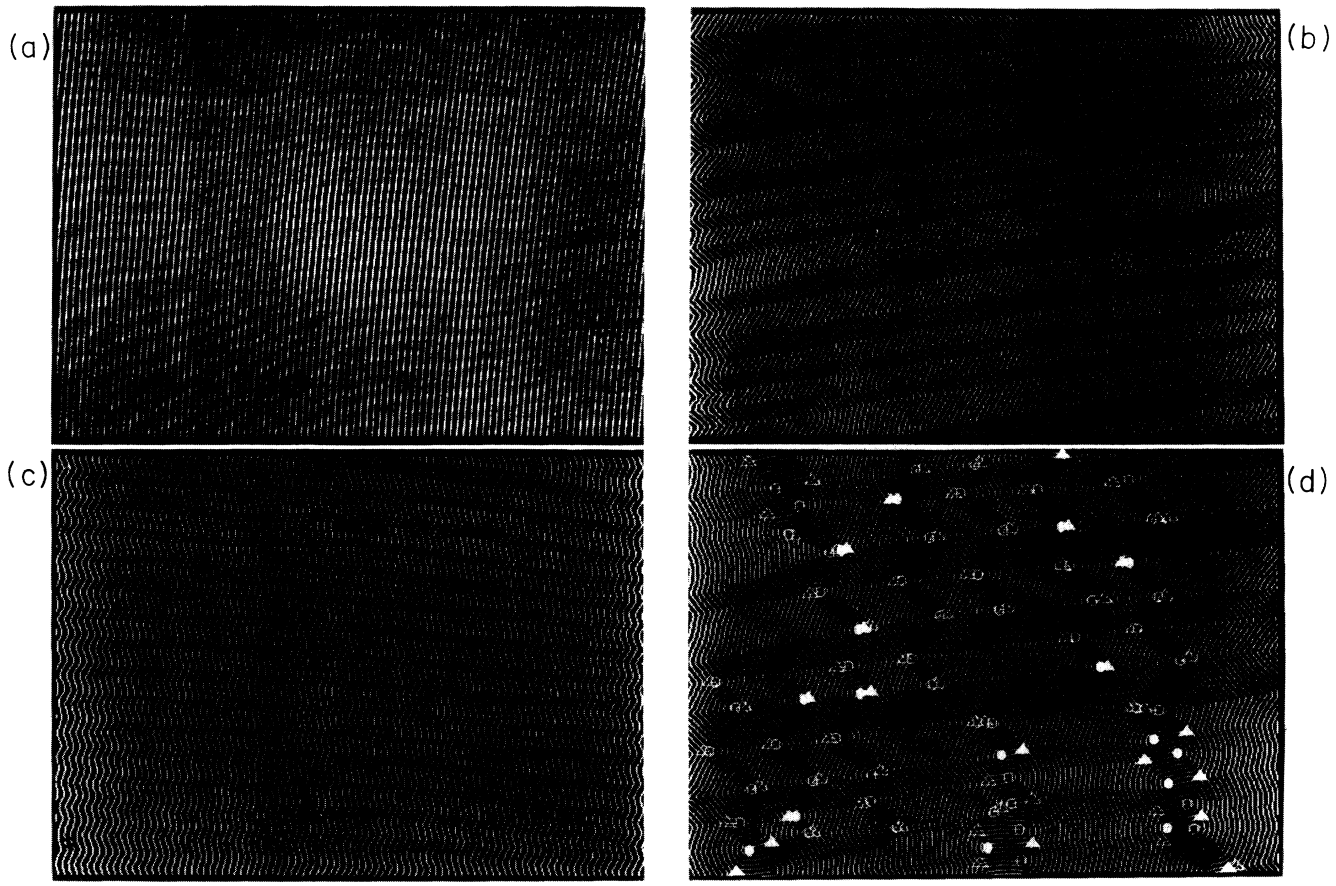

FIG. 8. Transverse ("smectic") instability of lamellar stripe pattern and nucleation of disclination dipoles, mediated by temperature-induced dilative strain. This figure represents a summary of the individual steps illustrated in Figs. 4 and 6. For clarity, only the medial axis transform [10] of the white component of the original image is shown in (b) (lower left), (c) (upper right), and (d) (lower right). In (d) topological defects in the form of branches and end points are marked by △, ▲, and ○, ●, respectively. The horizontal dimension of the field of view of each panel is 1.1 mm.

The sequence of smectic instabilities leading to the formation of topological defects is summarized in Fig. 8. Two distinct morphological motifs mark the defect-decorated chevron pattern in the lower panel of Fig. 6 and in Fig. 8(d), reflecting (imperfect) two-dimensionally periodic arrangements of disclination dipoles of differing symmetry. The first of these is visible in major portions of Fig. 6, which are occupied by a two-dimensional tiling of rhombohedral plaquettes. The plaquettes' vertices are marked by point dipoles of disclinations, as shown in Fig. 9: it should be noted in this context that a tightly bound pair of disclination charges is in fact equivalent to a free dislocation [37,60]. The configuration is reminiscent of that of free disclination charges marking the vertices of "quadrilaterals" or Lehmann clusters [see Fig. 9(b)], observed, for example, in cholesteric mesophases [59] and in the nematic phase of liquid crystalline polymers [61]. Quadrilaterals generally exist in isolation and display a shear instability leading to the pairwise annihilation of the decorating topological charges. This is in contrast to the periodic rhombohedral tiling observed here.

The formation of plaquettes involves the emergence of a new length scale set by the spacing of dipole pairs along the ridges of the parent chevron pattern. This length scale is identical to one lattice parameter a of each of the two interpenetrating rectangular sublattices occupied by point disclination dipoles of opposite orientation in what is equivalent to antiferromagnetic ordering on a centered rectangular lattice, as indicated in Figs. 9(c) and 9(d). The second lattice parameter b is identical to $\lambda_\perp$. In the symmetric geometry illustrated in Fig. 9(c), the local stripe segment orientation within a plaquette is orthogonal to the plaquette's long diagonal of length L, and one sees that $2\,a\sin(\hat{\alpha}/2)=L$. The second dimension, i.e., the plaquette's width W, is set by the dimensions of the parent chevron pattern, as may be ascertained from Fig. 9(c): $W=\lambda_\perp/2\sin(\hat{\alpha}/2)$. Note that requiring the identity of the lattice parameter a and the modulus of the displacement vector R_0, connecting the two rectangular sublattices decorated by defects and sketched in Fig. 9(c), in fact implies strictly threefold symmetry and hence $\hat{\alpha}=120°$, a condition we find to be only approximately met: As pointed out above, $110°\lesssim\hat{\alpha}\lesssim 115°$, as sketched in Fig. 9(d): Figure 8(d) suggests that in this case $a\simeq\lambda_\perp$, implying interpenetrating square sublattices.

The second motif realized in the defect-decorated chevron pattern of Fig. 6 is on more prominent display in Fig. 10. Linear arrays, or chains, of interdigitated disclination dipoles constitute the most striking structural feature in the arrangement, appearing as "zippered" cracks along which the original chevron pattern separates. It is apparent from the figure that these chains (or "cracks") are themselves ordered, thus forming a second two-dimensionally periodic defect pattern. Its symmetry, however, is distinct from and in fact lower than that of the earlier rhombohedral tiling: Rather than a centered rectangular, we now encounter an (essentially) rectangular unit cell, as sketched in Fig. 11. In significant contrast to the previous morphology based on point dipoles, disclination charges in a linear chain have already separated by a finite amount, forcing local alignment of

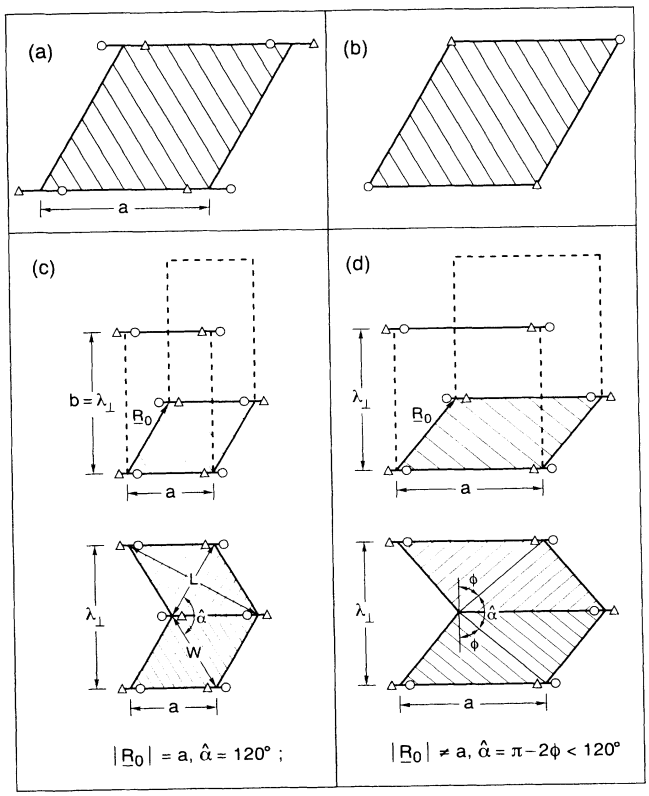

FIG. 9. Geometrical aspects of rhombohedral plaquettes, tiling stripe patterns which contain point dipoles of disclinations; this type of pattern is exemplified by Figs. 6 and 8. (a) shows the rhombohedral tile or plaquette: The relative orientations of stripes and disclination dipoles are indicated; dipoles are symbolized by a pair of branch and points: "△-○." For comparison, a Lehman cluster [61], or quadrilateral [58,59] decorated by disclinations, is sketched in (b). (c) and (d) illustrate the interpenetrating sublattices of disclination dipoles, characterized by a lattice parameter a and displacement vector R_0, as well as the actual tiling; the quantities W, L, a, and $\lambda_\perp$, as well as the angles ϕ and $\hat{\alpha}$, pertinent to the discussion in the text, are also indicated. (c) illustrates the symmetric case, $R_0=a$, $\hat{\alpha}=120°$, (d) the generally encountered situation in which $\hat{\alpha}<120°$.

the underlying stripe pattern with the linear segments connecting oppositely charged disclinations: As a result, a new local orientation emerges which is transverse to that of the original lamellar pattern of modulation wave vector $\mathbf{q}=(q_0,0)$.

As we will discuss in greater detail in II, the elongation of disclination dipoles represents a mechanism for strain relief which competes with the nucleation of additional defects, a process which is similarly strain induced. This is apparent in Figs. 6, 8(d), and 10, where linear chains of disclination dipoles are separated from one another by bands of intact chevron pattern of a characteristic width of $\hat{a}\simeq 2a$, where a, as defined in Fig. 9(c), denotes the spacing of point disclination dipoles along ridges of the parent chevron pattern. This implies that the density of

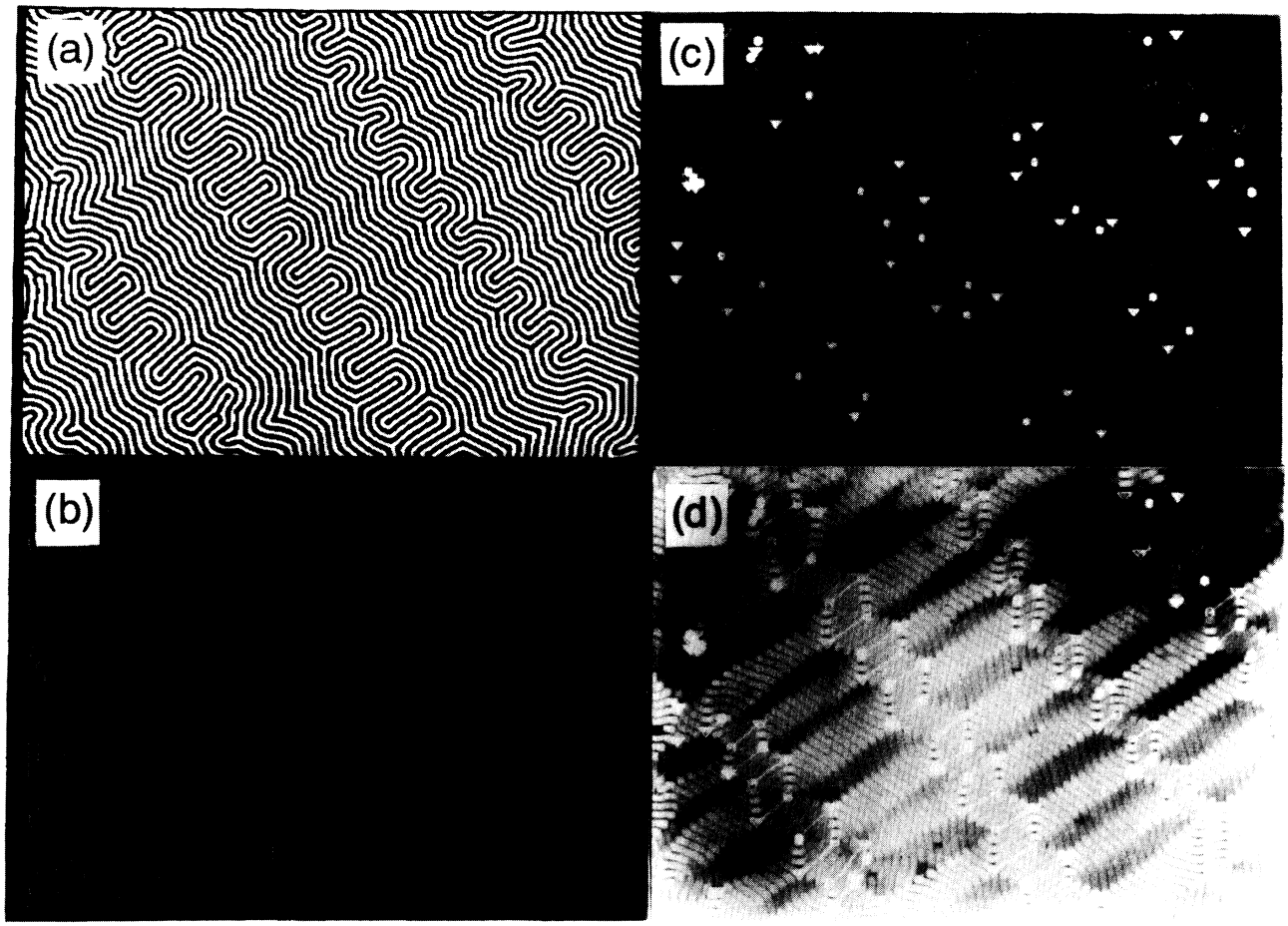

FIG. 10. Linear arrays of interdigitated disclination dipoles, generated from a chevron pattern such as that in the top panel of Fig. 6 or in Fig. 8(c). (a) (upper left) depicts the filtered original, (b) (lower left) the medial axis transform [10] of the white component of (a). (c) (upper right) contains the output of an algorithm designed to identify topological defects, notably $-\frac{1}{2}$ and $+\frac{1}{2}$ disclinations, in the pattern of (b): these are marked by "△," "▲," and "○," "●," respectively, open and solid symbols, referring, respectively, to the medial axis transforms of the white and black components of (a). Also displayed is the straight connecting line between opposite disclination charges paired into dipoles. (d) (lower right) represents the superposition of (c) and the original pattern, the latter treated by successive application of low-pass and dilation filters: The different gray shadings render visible regions of ordered, parallel stripe segments, further discussed in connection with Fig. 11. The horizontal dimension of each field of view is 905 μm.

defect pairs in the case of the rhombohedral plaquette tiling is significantly higher than in the case of the linear chain array where the pattern is tiled with essentially rectangular plaquettes. Estimating the respective areas of the quadrilateral primitive patches, we have, referring to Fig. 9(c), $A = LW = a\lambda_{\perp} \simeq \sqrt{3}a^2$ for the (symmetric) rhombus and, referring to Fig. 11, $A \simeq \lambda_{\perp} 2a \simeq 2\sqrt{3}a^2$ for the rectangle, suggesting defect densities to differ by a factor of approximately 2.

The balance between the two strain relief channels just introduced appears to be set by the rate of approaching the yield threshold of the chevron pattern, and by possible local variations in the strain distribution. In general, linear arrays form more easily and, once formed, represent the more stable morphology. In either case, a further increase in imposed strain leads to the "unbinding" of disclination pairs and the emergence of the globally disordered labyrinthine state. The full description of this process will be given in II. Intermediate states of disclination dipole "unbinding" in response to temperature-induced dilative strain are depicted in Fig. 12. Also shown is the final labyrinthine state, referred to as "branched" in companion articles focusing on its detailed structural analysis [9,10]. As in the precursor state, represented by the defect-decorated chevron pattern discussed above in connection with Figs. 8–11, disclinations are symmetrically distributed between bright and dark components of the labyrinthine pattern.

V. DISCUSSION

In Sec. IV we have addressed the evolution of disordered stripe domain states in ferrimagnetic garnet films, following an experimental trajectory originating in a

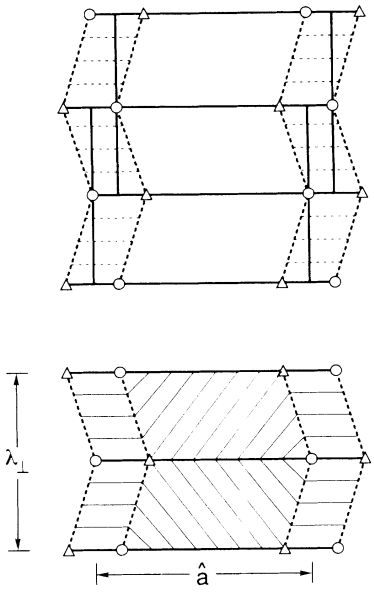

FIG. 11. Geometrical aspects of quadrilateral, nearly rectangular plaquettes, tiling stripe patterns which contain elongated declination dipoles; this type of pattern is exemplified by portions of Fig. 8(d) and particularly by Fig. 10. The quantities $\hat{a}$ and $\lambda_\perp$, pertinent to the discussion in the text, are also indicated. Note the appearance of a new motif in the form of staggered, short stripes parallel to the elongated disclination dipoles, "△-○." The actual tiling is illustrated in the lower sketch.

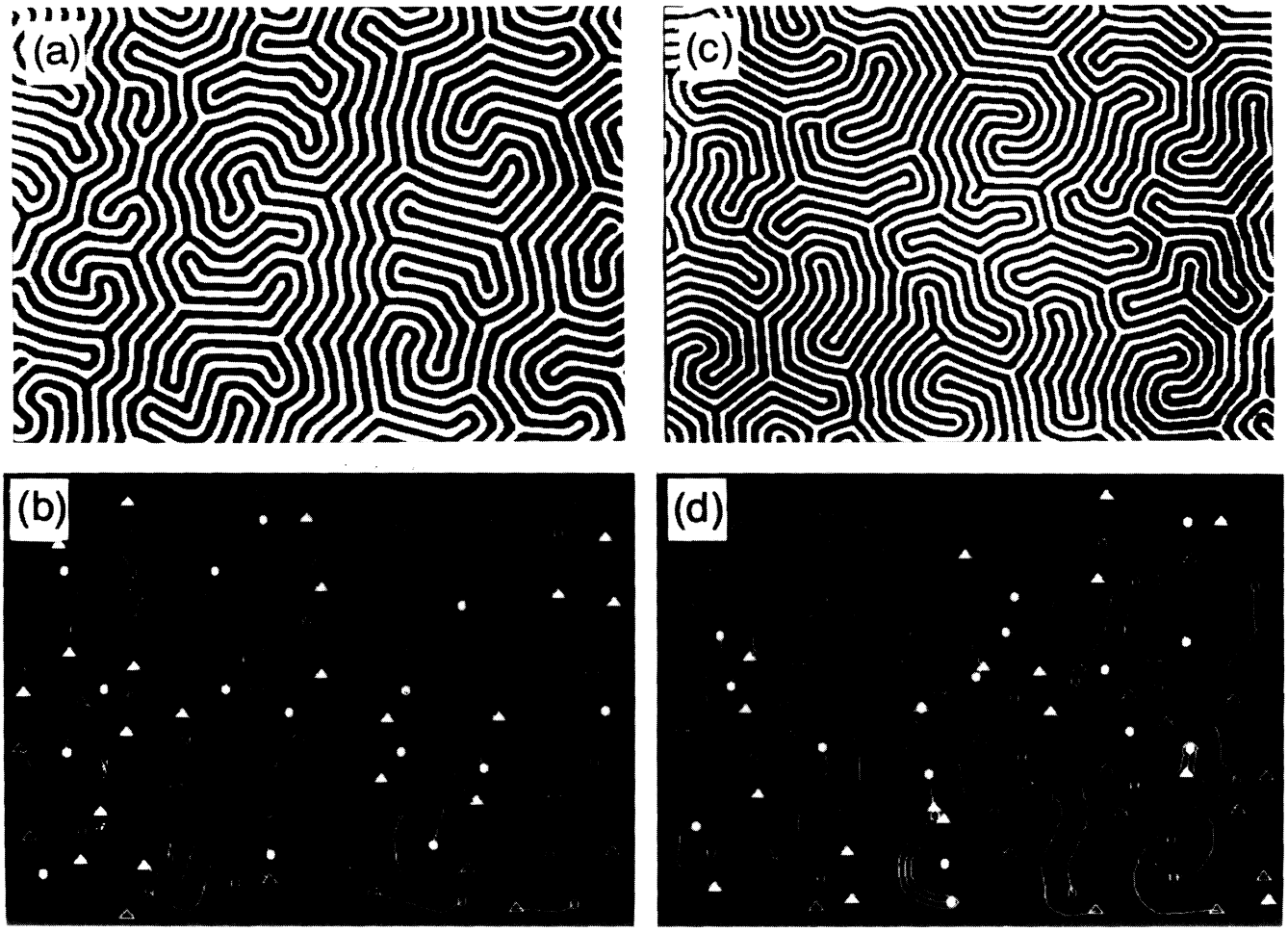

FIG. 12. Snapshots depicting intermediate states in the course of disclination dipole unbinding in response to temperature-induced dilative strain, leading to the evolution of a "branched" labyrinthine pattern; $H=0$ Oe. The top panels show binarized patterns: For the pattern on the left: $T=134\,^{\circ}\mathrm{C}$ ($\simeq 0.7T_c$), stripe period, $d=13$ μm; for the pattern on the right: $T=160\,^{\circ}\mathrm{C}$ ($\simeq 0.8T_c$), $d=11$ μm. The bottom panels exhibit disclinations of opposite sign ("△," "▲": $-\frac{1}{2}$; "○," "●": $+\frac{1}{2}$) as well as their connecting tethers [9,10], as extracted from the respective original patterns on top; open and solid symbols mark, respectively, disclinations in the white and dark components. The horizontal dimension of each field of view is 570 μm.

lamellar initial state, characterized by a given $d=d(T_0)=d_0$ and $m=0$, and coinciding with the $H=0$ symmetry axis in the mean-field phase diagram. This trajectory is traversed by tuning the modulation period $d=d(H,T)$ of the pattern via its temperature dependence, as discussed in Sec. III. For the garnets studied here to maintain the ordered lamellar stripe configuration of globally minimal free energy requires the equivalent adjustment in the number of lamellae. That is, the "correct" number of lamellae N_L must satisfy the condition $N_L \simeq L_0/d$, L_0 denoting the linear sample dimension. While such a process in the form of "ejection" of lamellae is in fact observed when increasing the period, as illustrated in Fig. 3, the analogous "injection" of additional lamellae, requiring a suitable nucleation event, is suppressed. That is, downward and upward period adjustments are mediated by completely different processes. The requisite period reduction implied by raising temperature along the $H=0$ symmetry axis must proceed under the constraint of maintaining constant the number of lamellae present, while simultaneously filling the available area, $A_0 \simeq L_0^2$ with a stripe pattern of minimal free energy which exhibits the required period d as well as the correct stripe width, realizing the correct magnetization m. The resulting disordered stripe patterns thus represent the solution to a problem of constrained optimization. Equivalently, they correspond to the minimization of a Helmholtz rather than a Gibbs free energy.

The initial smectic elastic response to the accumulation of dilative strain leads to undulation and chevron patterns, exhibiting curvature and discontinuity walls, respectively. The primary transverse instability generating the undulation pattern appears to conform to the picture suggested by the effective elastic theory described in Sec. III [19]. Within the framework of this local theory, the instability is equivalent to that of a smectic-A liquid crystal of N layers confined between parallel glass plates and subjected to mechanical stress [56,57]. This strongly suggests that, while nonlocal interactions are crucial in setting the modulation period for given magnetic field and temperature, the response to changes in this optimal value is well described by a local elastic theory. The strong resistance to longitudinal layer compression favors bending, characterized by a transverse period $\lambda_\perp$, a situation analogous to that encountered with liquid crystals and quite probably with related materials such as diblock copolymers in their lamellar state. Optical diffraction demonstrates the continuous evolution of the undulation into the chevron pattern. This evolution results in the concentration of curvature energy in discontinuity walls. This evolution, particularly the period doubling observed within the chevron superstructure, likely representing a highly nonlinear elastic response, is presently not fully accounted for by theory, but may have more general significance. For example, the electron-microscopic investigation of "ripple" phases in certain lamellar lyotropic liquid crystals reveals the frequent coexistence of two ripple periods related by a factor of approximately 2 [62]. Significant strain, arising from the downward adjustment of the lamellar repeat distance, or layer period, required in response to heating, may accumulate, in a manner related to what has been presented here.

The chevron pattern eventually becomes unstable with respect to the formation of disclination dipoles, oriented perpendicular to the original lamellar pattern: This process of nucleating additional lamellae by way of line branching ("pincements" [59]) serves as a mechanism of strain relief. The emerging "tethers" connect disclination charges of opposite sign. The subsequent topologically constrained disclination dipole unbinding also constitutes a form of stripe elongation and we show in II that this observation suggests a simple scaling argument describing the dependence of the contour length of the injected segments on dilative strain.

We have characterized the process of disordering by focusing explicitly on topological point defects, notably disclinations. A full discussion of this topic is more suitably undertaken in II on the basis of an additional set of data on the evolution of labyrinthine patterns in response to magnetic-field-induced strain.

ACKNOWLEDGMENTS

L. Monar's technical contributions in constructing experimental apparatus are gratefully acknowledged. Various aspects of the work described here have benefited from a number of useful conversations with E. Bodenschatz, S. Hudson, D. Huse, D. Nelson, L. O'Gorman, and S. Singer.

[1] M. Seul and D. Andelman (unpublished).
[2] T. Mitsui and J. Furuichi, Phys. Rev. **90**, 193 (1953).
[3] T. F. Faber, Proc. R. London, Ser. A **248**, 460 (1958).
[4] R. Rosensweig, *Ferrohydrodynamics* (Cambridge University Press, Cambridge, 1982). Chap. 7.
[5] C. Kooy and U. Enz, Philips Res. Rep. **15**, 7 (1960).
[6] H. M. McConnell, Annu. Rev. Phys. Chem. **41**, 171 (1991).
[7] M. Seul and M. J. Sammon, Phys. Rev. Lett. **64**, 1903 (1990); M. Seul, Physica A **168**, 198 (1990).
[8] M. Seul and R. Wolfe, Phys. Rev. Lett. **68**, 2460 (1992).
[9] M. Seul, L. R. Monar, L. O'Gorman, and R. Wolfe, Science **254**, 1616 (1991).
[10] M. Seul, L. R. Monar, and L. O'Gorman, Philos. Mag. B **66**, 471 (1992).
[11] M. Kléman, *Points, Lines and Walls* (Wiley, New York, 1983).
[12] M. Seul, M. J. Sammon, and L. R. Monar, Rev. Sci. Instrum. **62**, 784 (1991).
[13] A. Tardieu, V. Luzzati, and F. C. Reman, J. Mol. Biol. **75**, 711 (1973).
[14] F. S. Bates and G. H. Fredrickson, Annu. Rev. Phys. Chem. **41**, 525 (1990).
[15] R. E. Rosensweig, M. Zahn, and R. J. Shumovich, J. Magn. Magn. Mater. **39**, 127 (1983).
[16] J. A. Cape and G. W. Lehman, J. Appl. Phys. **42**, 5732

(1971).
[17] O. L. Alerhand, D. Vanderbilt, R. D. Meade, and J. D. Joannopoulos, Phys. Rev. Lett. **61**, 1973 (1988).
[18] T. Garel and S. Doniach, Phys. Rev. B **26**, 325 (1982).
[19] D. Sornette, J. Phys. (Paris) **48**, 151 (1987); **48**, 1413 (1987).
[20] W. A. Barker and G. A. Gehring, J. Phys. C **16**, 6415 (1983).
[21] L. Landau and E. M. Lifshitz, *Electrodynamics of Continuous Media* (Pergamon, New York, 1959), Vol. VIII, Chap. 39.
[22] Z. Malek and V. Kambersky, Czech. J. Phys. **8**, 16 (1958).
[23] M. Seul and R. Wolfe (unpublished).
[24] C. Kittel, Phys. Rev. **70**, 965 (1946); Rev. Mod. Phys. **21**, 541 (1949).
[25] L. N. Bulaevskii and V. L. Ginzburg, Zh. Eksp. Teor. Fiz. **45**, 772 (1963) [Sov. Phys.—JETP **18**, 530 (1964)].
[26] J. W. Cahn, J. Chem. Phys. **66**, 3667 (1977).
[27] A. H. Eschenfelder, *Magnetic Bubble Technology* (Springer-Verlag, Berlin, 1980).
[28] T. H. O'Dell, Rep. Prog. Phys. **49**, 509 (1986).
[29] S. Konishi, IEEE Trans. Mag. **MAG-19**, 1838 (1983).
[30] K. L. Babcock and R. M. Westervelt, Phys. Rev. Lett. **63**, 175 (1989); **64**, 2168 (1990); Phys. Rev. A **41**, 1952 (1990).
[31] D. Weaire, F. Bolton, P. Molho, and J. A. Glazier, J. Phys. Condens. Matter **3**, 2101 (1991).
[32] J. A. Glazier, S. P. Gross, and J. Stavans, Phys. Rev. A **36**, 306 (1987).
[33] R. Seshadri and R. M. Westervelt, Phys. Rev. Lett. **66**, 2775 (1991).
[34] P. Molho, J. L. Porteseil, and Y. Souche, J. Appl. Phys. **63**, 4327 (1988).
[35] P. Molho, J. L. Porteseil, Y. Souche, J. Gouzerh, and J. C. S. Levy, J. Appl. Phys. **61**, 4188 (1987).
[36] J. Toner and D. R. Nelson, Phys. Rev. B **23**, 316 (1981).
[37] D. R. Nelson and J. Toner, Phys. Rev. B **24**, 363 (1981).
[38] W. Helfrich, Z. Naturforsch., Teil A **33**, 305 (1978).
[39] D. Roux and C. R. Safinya, J. Phys. (Paris) **49**, 307 (1988); G. Porte, J. Appell, P. Basserau, and J. Marignan, *ibid.* **50**, 1335 (1990).
[40] B. I. Halperin, in *Physics of Defects,* Les Houches, Session XXXV, 1980 edited by R. Balian *et al.* (North-Holland, Amsterdam, 1981), Chap. 14.
[41] K. J. Strandburg, Rev. Mod. Phys. **60**, 161 (1988).
[42] S. Ostlund and B. I. Halperin, Phys. Rev. B **23**, 335 (1981).
[43] J. Als-Nielsen, J. D. Litster, R. J. Birgeneau, M. Kaplan, C. R. Safinya, A. Lindegaard-Andersen, and S. Mathiesen, Phys. Rev. B **22**, 312 (1980).
[44] D. R. Nelson and R. A. Pelcovits, Phys. Rev. B **16**, 2191 (1977).
[45] S. G. J. Mochrie, A. R. Kortan, R. J. Birgeneau, and P. M. Horn, Phys. Rev. Lett. **53**, 985 (1984); Z. Phys. B **62**, 79 (1985).
[46] D. E. Moncton, P. W. Stephens, R. J. Birgeneau, P. M. Horn, and G. S. Brown, Phys. Rev. Lett. **46**, 1533 (1981); **49**, 1679 (1982); P. W. Stephens, P. A. Heiney, R. J. Birgeneau, P. M. Horn, D. E. Moncton, and G. S. Brown, Phys. Rev. B **29**, 3512 (1984).
[47] K. Kjaer, M. Nielsen, J. Bohr, H. J. Lanter, and J. P. McTague, Phys. Rev. B **26**, 5168 (1982).
[48] J. F. Sadoc and R. Mosseri, in *Topological Disorder in Condensed Matter,* edited by F. Yonezawa and T. Ninomiya, (Springer-Verlag, Berlin, 1983), p. 30.
[49] D. R. Nelson, Phys. Rev. B **28**, 5515 (1983).
[50] R. Zallen, in *Fluctuation Phenomena,* edited by E. W. Montroll and J. L. Lebowitz (North-Holland, Amsterdam, 1979), Chap. 3.
[51] N. Rivier and D. M. Duffy, J. Phys. (Paris) **43**, 293 (1982).
[52] N. Rivier, in *Topological Disorder in Condensed Matter,* edited by F. Yonezawa and T. Ninomiya (Spring Verlag, Berlin, 1983), p. 14.
[53] S. C. Moss and D. L. Price, in *Physics of Disordered Materials,* edited by D. Adler, H. Fritzsche, and S. R. Ovshinsky (Plenum, New York, 1985), p. 77.
[54] P. H. Gaskell, M. C. Eckersley, A. C. Barnes, and P. Chieux, Nature **350**, 675 (1991).
[55] A. Weber, E. Bodenschatz, and L. Kramer, Adv. Mater. **3**, 191 (1991).
[56] N. A. Clark and R. B. Meyer, Appl. Phys. Lett. **22**, 493 (1973); R. Ribotta and G. Durand, J. Phys. (Paris) **38**, 179 (1977).
[57] Ch. S. Rosenblatt, R. Pindak, N. A. Clark, and R. B. Meyer, J. Phys. (Paris) **38**, 1105 (1977); N. A. Clark and A. J. Hurd, *ibid.* **43**, 1159 (1982).
[58] M. Kléman, in *Dislocations in Solids,* edited by F. R. N. Nabarro (North-Holland, Amsterdam, 1980), Vol. 5, Chap. 22.
[59] Y. Bouligand, in *Dislocations in Solids,* edited by F. R. N. Nabarro (North-Holland, Amsterdam, 1980), Vol. 5, Chap. 23.
[60] D. R. Nelson, Phys. Rev. B **26**, 269 (1982).
[61] B. A. Wood and E. L. Thomas, Nature **324**, 655 (1986); S. D. Hudson and E. N. Thomas, Phys. Rev. A **44**, 8128 (1991).
[62] J. A. Zasadzinski and M. B. Schneider, J. Phys. (Paris) **48**, 2001 (1987).

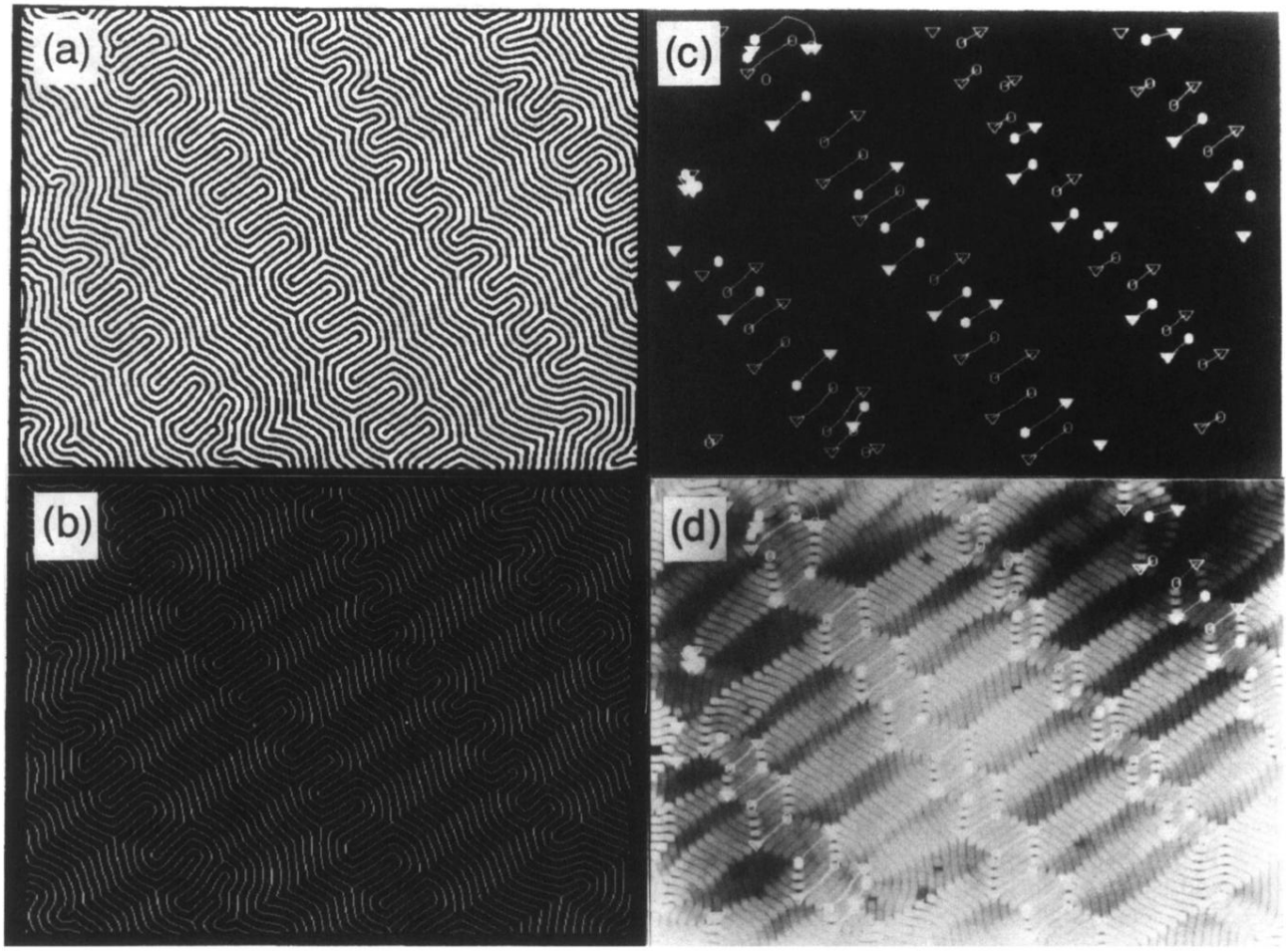

FIG. 10. Linear arrays of interdigitated disclination dipoles, generated from a chevron pattern such as that in the top panel of Fig. 6 or in Fig. 8(c). (a) (upper left) depicts the filtered original, (b) (lower left) the medial axis transform [10] of the white component of (a). (c) (upper right) contains the output of an algorithm designed to identify topological defects, notably $-\frac{1}{2}$ and $+\frac{1}{2}$ disclinations, in the pattern of (b): these are marked by "△," "▲," and "○," "●," respectively, open and solid symbols, referring, respectively, to the medial axis transforms of the white and black components of (a). Also displayed is the straight connecting line between opposite disclination charges paired into dipoles. (d) (lower right) represents the superposition of (c) and the original pattern, the latter treated by successive application of low-pass and dilation filters: The different gray shadings render visible regions of ordered, parallel stripe segments, further discussed in connection with Fig. 11. The horizontal dimension of each field of view is 905 μm.

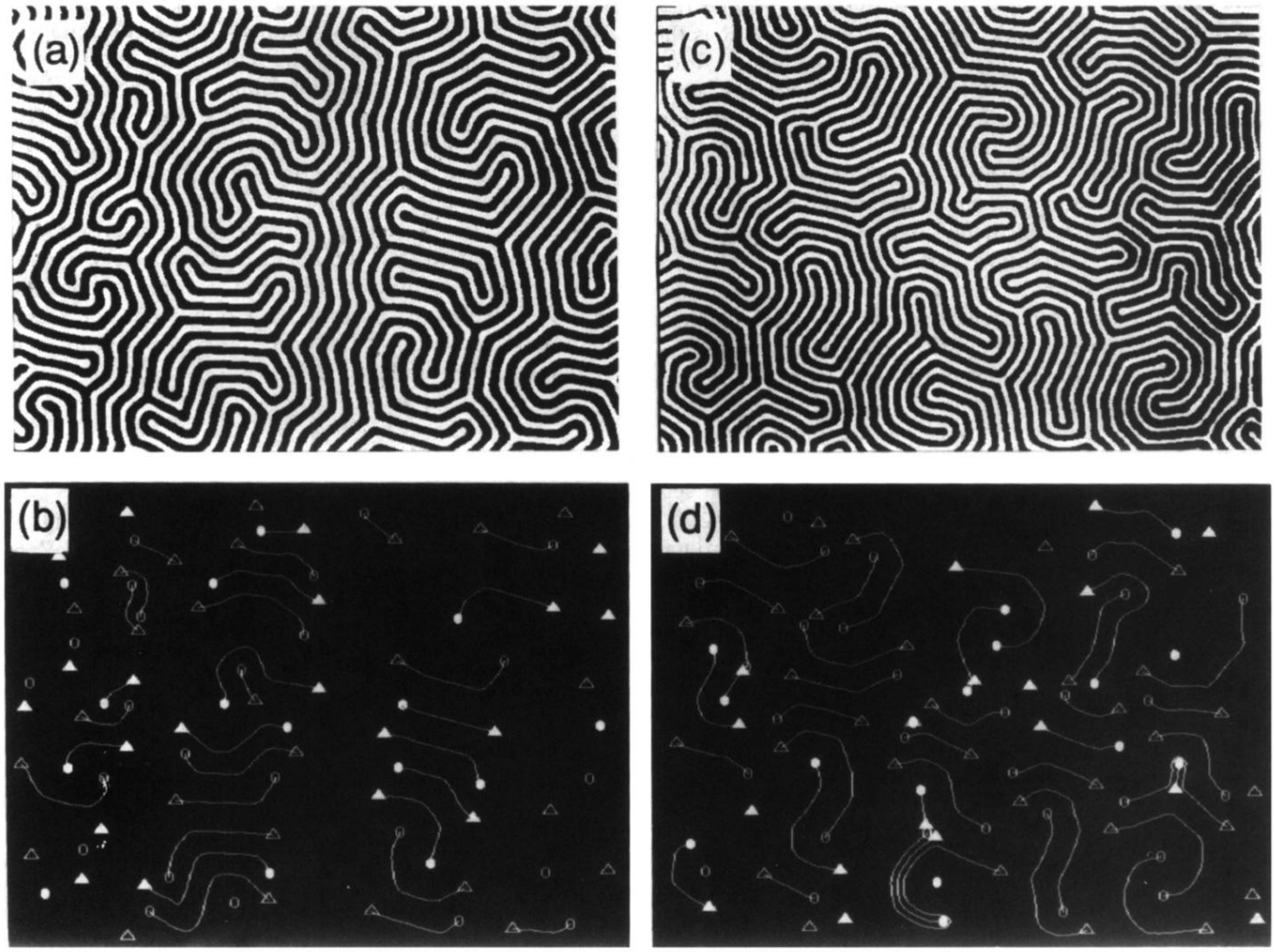

FIG. 12. Snapshots depicting intermediate states in the course of disclination dipole unbinding in response to temperature-induced dilative strain, leading to the evolution of a "branched" labyrinthine pattern; $H=0$ Oe. The top panels show binarized patterns: For the pattern on the left: $T=134\,^{\circ}\mathrm{C}$ ($\simeq 0.7T_c$), stripe period, $d=13\ \mu$m; for the pattern on the right: $T=160\,^{\circ}\mathrm{C}$ ($\simeq 0.8T_c$), $d=11\ \mu$m. The bottom panels exhibit disclinations of opposite sign ("△," "▲": $-\frac{1}{2}$; "○," "●": $+\frac{1}{2}$) as well as their connecting tethers [9,10], as extracted from the respective original patterns on top; open and solid symbols mark, respectively, disclinations in the white and dark components. The horizontal dimension of each field of view is 570 μm.

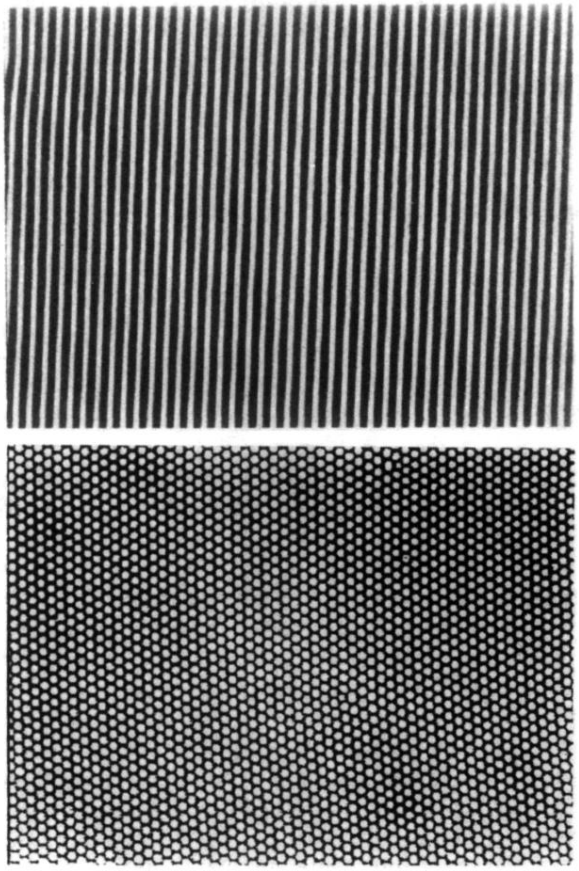

FIG. 2. Experimental examples of (spontaneously formed) "stripe" and "bubble" phases, recorded in a ferrimagnetic garnet film of the type investigated here and described in Sec. II of the text. Field and temperature settings were $H=0$ Oe, $T\simeq 0.6T_c$ and $H=5$ Oe, $T\simeq 0.9T_c$, respectively, for stripe and bubble patterns; $T_c\simeq 192\,^{\circ}\mathrm{C}$. The horizontal dimension of the field of view is 570 μm in both cases.

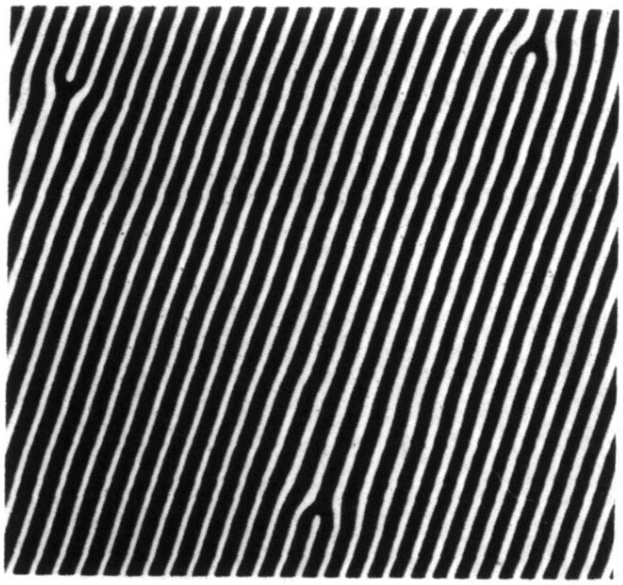

FIG. 3. Snapshot of dislocation climb, observed in the course of cooling a lamellar stripe pattern along the $H=0$ axis of the phase diagram of Fig. 1: This process of "ejecting" stripes enables the pattern to accommodate the increase in the stripe period induced by lowering the temperature, as discussed in Sec. IV A of the text. The horizontal dimension of the field of view is 930 μm; the stripe period is 32 μm.

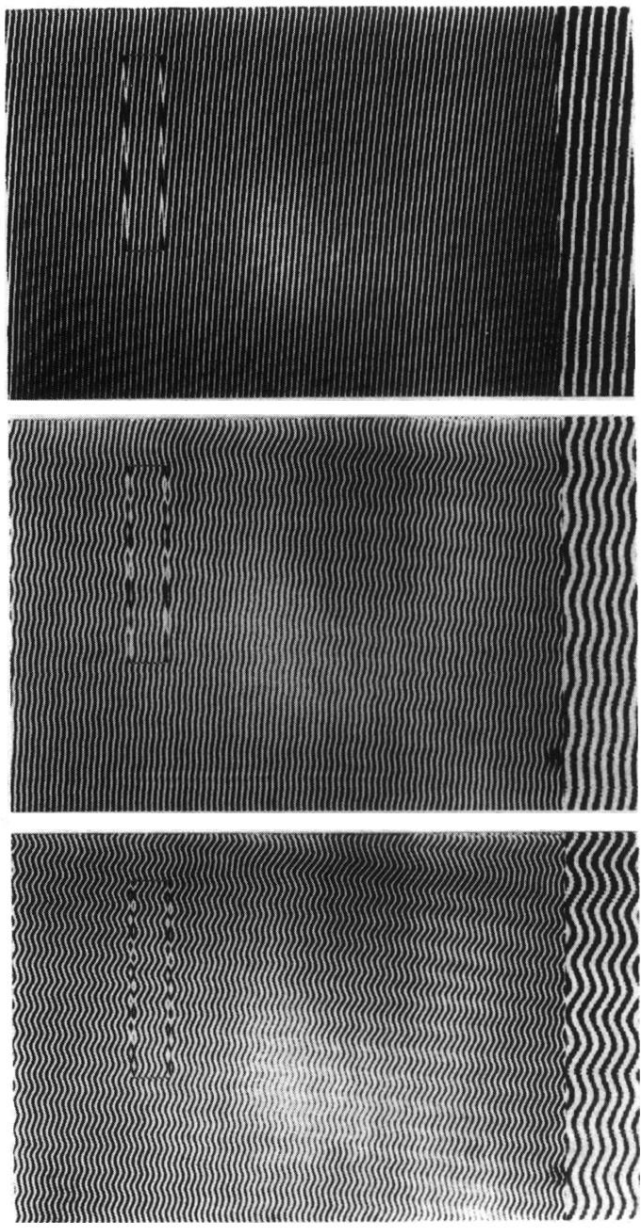

FIG. 4. Undulation instability of lamellar stripe pattern; the instability is induced by dilative strain, generated by heating along the $H=0$ axis of the phase diagram of Fig. 1(a). The lamellar initial state is displayed in the top panel. The transient depicted in the middle panel suggests that amplitude growth (along each undulating stripe) is continuous. The fully evolved undulation is shown in the bottom panel. The original images were processed by successive application of low-pass and high-pass filters. For clarity the vertical panel on the right-hand side of each figure depicts a twofold magnified view of the portion delineated by the rectangular box in the original. The horizontal dimension of the original field of view is 1.2 mm.

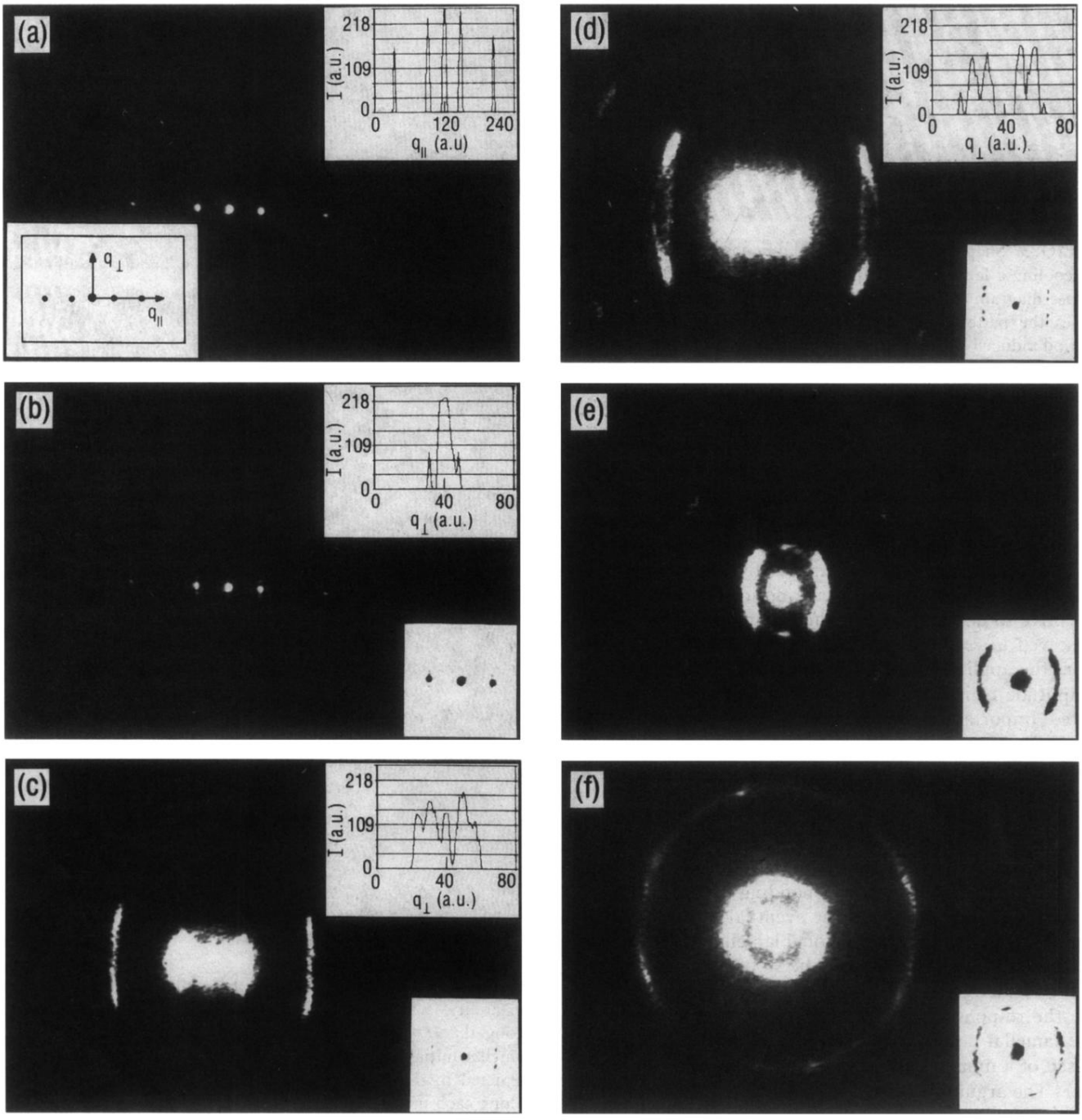

FIG. 5. Optical diffraction patterns characterizing transverse instability of lamellar pattern, the resulting undulation and chevron patterns, and the appearance of disclination dipoles and their subsequent unbinding (see further discussion in the text). The limiting ratio $q_{\perp}/q_{\parallel}=q_{\perp}/q_0=0.71$, realized in the chevron pattern giving rise to the spectrum in D, implies a substantial strain, $\epsilon=(d_0-d)/d_0=1-1/[1+(q_{\perp}/q_0)^2]^{1/2}=0.18$. Insets contain resolved recordings of the central portion of the pattern in (b)–(f), as well as longitudinal (a) and transverse scans (b)–(d), the latter centered at the (10) position.

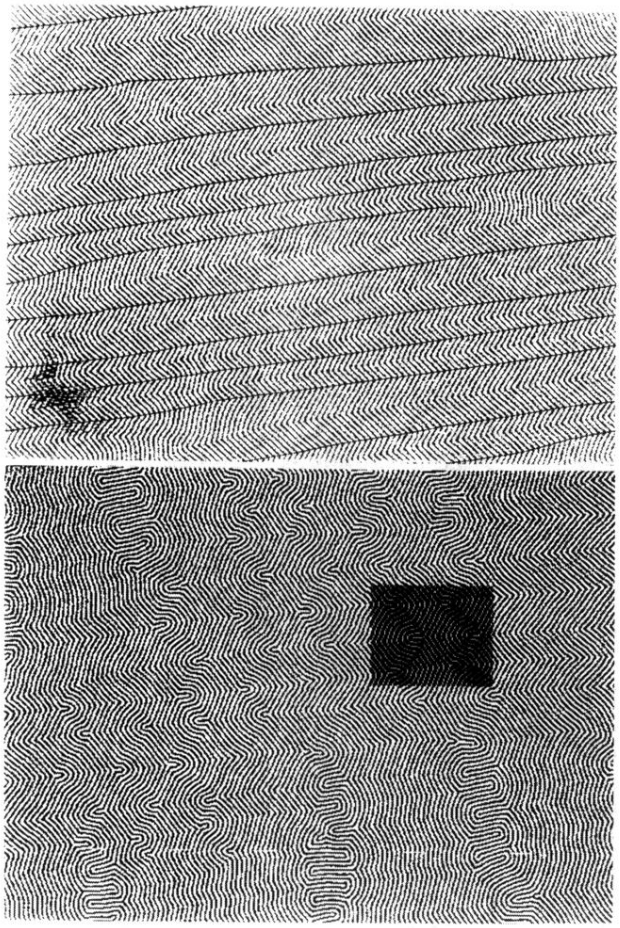

FIG. 6. Chevron pattern (top) and emerging disclination dipole pairs (bottom). Right-pointing cusps in the chevron pattern are connected by a thin line to guide the eye. The highlighted portion of the bottom photograph contains the medial axis transform [10], or "skeleton," of the white component and illustrates the appearance of rhombohedral tiles with defect-decorated vertices, as discussed in the text [(see also Fig. 8(d)]. The original images were processed by successive application of low-pass and high-pass filters. The horizontal dimension of the field of view is 1.4 mm.

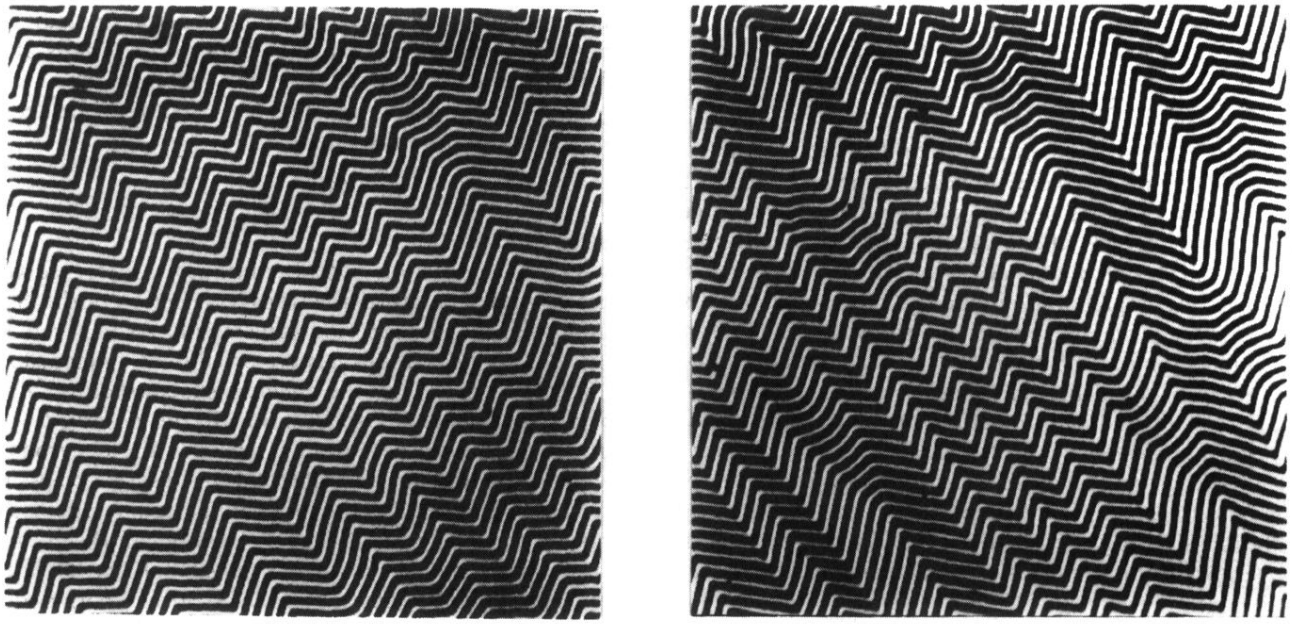

FIG. 7. Edge ("meta") dislocations in the array of discontinuity walls defining a chevron pattern of the type shown in the top panel of Fig. 6. These defects appear to mediate the period adjustment in the chevron pattern in a manner analogous to the process discussed in connection with Fig. 3. The horizontal dimension of each field of view is approximately 690 μm.

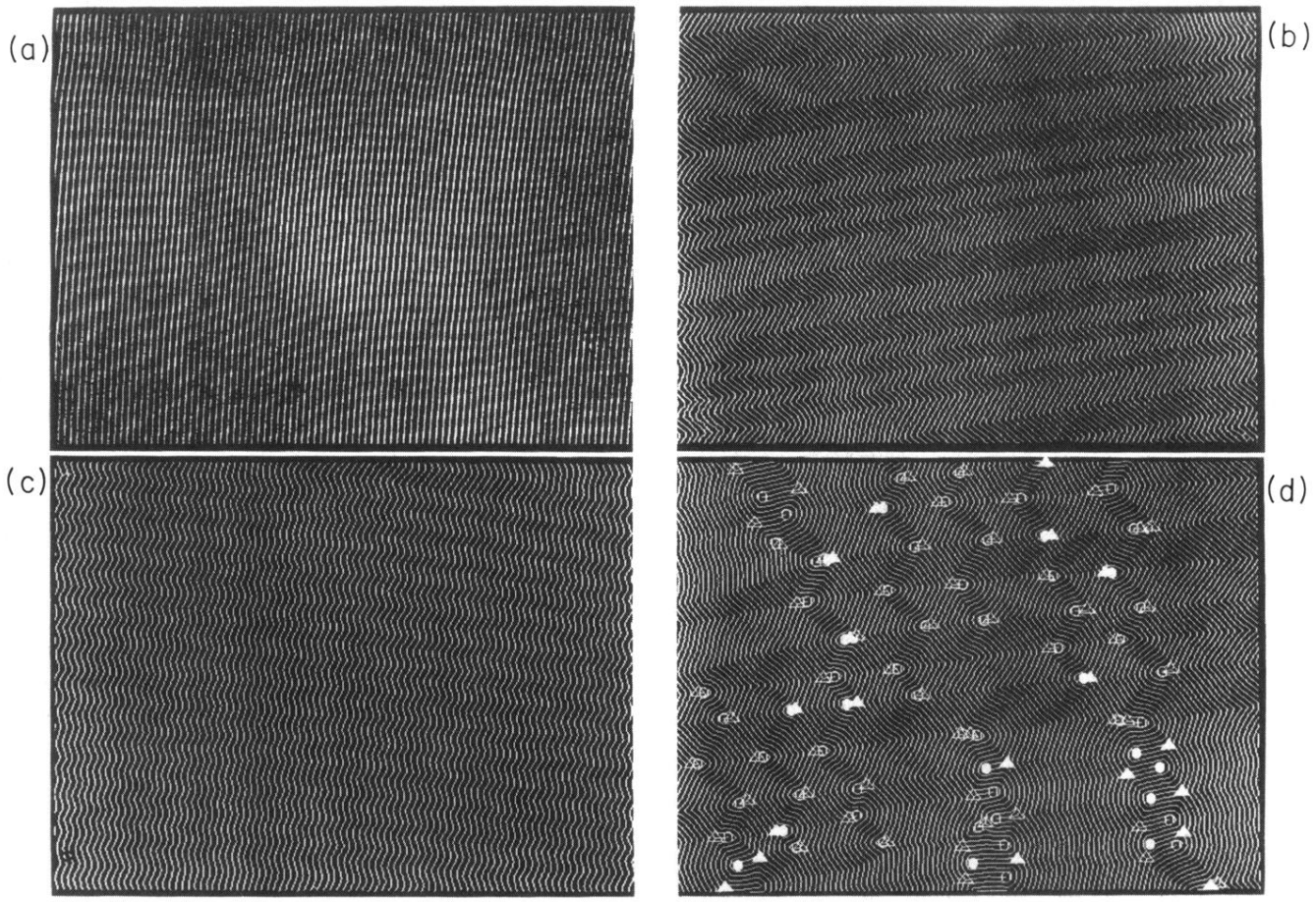

FIG. 8. Transverse ("smectic") instability of lamellar stripe pattern and nucleation of disclination dipoles, mediated by temperature-induced dilative strain. This figure represents a summary of the individual steps illustrated in Figs. 4 and 6. For clarity, only the medial axis transform [10] of the white component of the original image is shown in (b) (lower left), (c) (upper right), and (d) (lower right). In (d) topological defects in the form of branches and end points are marked by △, ▲, and ○, ●, respectively. The horizontal dimension of the field of view of each panel is 1.1 mm.